Biophysical Journal Volume 74 February 1998 1043–1060

Trapping and Wiggling: Elastohydrodynamics of Driven Microfilaments

Chris H. Wiggins,* D. Riveline,# A. Ott,# and Raymond E. Goldstein§

*Department of Physics, Princeton University, Princeton, New Jersey 08544 USA; #Institut Curie, Section de Physique et Chimie, 75231 Paris Cedex 05, France; and §Department of Physics and Program in Applied Mathematics, University of Arizona, Tucson, Arizona 85721 USA

ABSTRACT We present an analysis of the planar motion of single semiflexible filaments subject to viscous drag or point forcing. These are the relevant forces in dynamic experiments designed to measure biopolymer bending moduli. By analogy with the "Stokes problems" in hydrodynamics (motion of a viscous fluid induced by that of a wall bounding the fluid), we consider the motion of a polymer, one end of which is moved in an impulsive or oscillatory way. Analytical solutions for the time-dependent shapes of such moving polymers are obtained within an analysis applicable to small-amplitude deformations. In the case of oscillatory driving, particular attention is paid to a characteristic length determined by the frequency of oscillation, the polymer persistence length, and the viscous drag coefficient. Experiments on actin filaments manipulated with optical traps confirm the scaling law predicted by the analysis and provide a new technique for measuring the elastic bending modulus. Exploiting this model, we also present a reanalysis of several published experiments on microtubules.

INTRODUCTION

Attempts by theoretical physicists to contribute in some useful way to the study of biology have, so far, been most successful in systems in which all forces and motion can be modeled and mathematized explicitly, or in those governed by equilibrium statistical mechanics, for which equipartition can be invoked. One specific example of such success is the analysis of structural microfilaments, essentially one-dimensional mechanical objects with no moving parts. Despite this unassuming mechanical description, these semiflexible biopolymers are essential for innumerable functions and processes at the molecular and cellular level.

Depending on the bending modulus of the filament in question, experiments investigating the elastic properties of these biopolymers largely rely on either mechanical or statistical techniques. Microtubules, with a persistence length of ~5 mm, are quite amenable to micromanipulation or forcing via hydrostatic drag. Actin and nucleic acids, with persistence lengths near 15 μm and 50 nm, respectively, fall in the realm of statistical mechanics (note that we are here addressing the bending elasticity, not the stretching elasticity, another area of great excitement and successes; Yin et al., 1995; Cluzel et al., 1996; Smith et al., 1996).

An area in which careful analysis has been less prevalent, however, is investigations of dynamics at the single polymer level. Such a theoretical program has only recently been made experimentally relevant through the advent of optical tweezers and the proliferation of similar techniques for precise and controllable micromanipulation. Whereas treatments of the undamped, inertial case have a long history (Harris and Hearst, 1966; Landau and Lifshitz, 1986), and viscously overdamped dynamics have been studied in great detail and with exciting results in bulk for polymer gels (Isambert and Maggs, 1996; MacKintosh and Janmey, 1997), the application of viscous dynamics to single polymers and connections with experiment have not been fully elucidated. We intend this paper to be a complement to the important works done in the inertial and bulk contexts.

Specifically, we here couple elasticity theory and overdamped viscous hydrodynamics (as is appropriate in the biological context) to explore elastohydrodynamics. Although equations with the appropriate units will be sufficient to determine the scales of forces and velocities, if we wish to extract numbers from the experiments it is necessary to perform a thorough analysis. The slenderness of the filaments allows us to simplify greatly the hydrodynamics and arrive at a local partial differential equation of motion. We find that coupling to hydrodynamics allows us to extend the range of mechanical experiments to much smaller bending moduli. For example, whereas measurements of actin's rigidity so far have been via fluctuation analyses invoking equipartition and thus statistical mechanics, we present here an experimental method that does not rely on nonzero temperature. Furthermore, the method allows investigation into questions that have been raised about whether actin can even be treated as a semiflexible polymer, or is in fact scale-sensitive (Käs et al., 1993) or dynamic in its elasticity. Such a purely mechanical treatment obviates the possible complications of statistical treatments like dimensionality (Ott et al., 1993), correlations among sampled images, or self-avoidance.

It is our hope that this new experimental method, as well as the general analytic techniques here outlined, will contribute to the current exciting and active dialogue among physicists and biologists regarding the nature and numbers behind biopolymer rigidity, as well as the effects of associated proteins and varying biochemical environments on elastic moduli. Furthermore, these new methods and anal-

Received for publication 2 April 1997 and in final form 6 November 1997.

Address reprint requests to Chris Wiggins, Department of Physics, University of Arizona, Tucson, AZ 85721. Tel.: 520-621-6798; Fax: 520-621-4721; E-mail: cwiggins@princeton.edu.

0006-3495/98/02/1043/18 $2.00

yses should prove useful in the study of other examples of dynamic elastic filaments, such as supercoiled fibers of *B. subtilis* (Mendelson, 1990). We intend this investigation to be the necessary precursor to such promising extensions.

A useful starting point for developing the dynamics of an elastic filament in a viscous medium will be to consider the simplest time dependencies possible. To that end, recall the classic problems introduced by G. G. Stokes (Stokes, 1851), illustrated in Fig. 1, involving the motion of a viscous fluid bounded by a wall that is either (I) moved impulsively or (II) oscillated. These easily solvable problems capture the essential ideas of viscous diffusion of velocity. The experimental geometry is such that the Navier-Stokes equation for the velocity field $u(x, t)$ is simply the diffusion equation

$$u_t = \nu u_{xx} \tag{1}$$

where $\nu = \mu/\rho$ is the kinematic viscosity, and μ and ρ are the fluid viscosity and density. Subscripts on functions indicate differentiation throughout unless otherwise indicated. The salient features of the solutions are the relationships between length scales, time scales, and material parameters. Specifically, in the impulsive case, the velocity at any point x and time t depends only on the ratio $x/(\nu t)^{1/2}$; likewise, in the oscillatory case, deformations decay with a characteristic length that scales as $\ell_S(\omega) = (\nu/\omega)^{1/2}$.

We introduce here the analogous two problems in elastohydrodynamics, illustrated in Fig. 2. They involve (I) the deflection of a polymer anchored at one end after the instantaneous introduction of a uniform fluid velocity U, and (II) the steady undulations of a polymer, one end of which is oscillated. Rather than a diffusion equation as in the Stokes problems, the dynamics of small deformations $y(x, t)$ of the filament are governed by a fourth-order partial differential equation of the form

$$y_t = -\tilde{\nu} y_{xxxx} \tag{2}$$

where $\tilde{\nu} = A/\zeta$ plays the role of a "hyperdiffusion" coefficient, A is the bending modulus, and ζ is the drag coefficient. This equation has appeared before in the literature on semiflexible biopolymers (Barkley and Zimm, 1978; Amblard et al., 1996; Gittes et al., 1993), primarily in the context of scaling arguments for relaxation times; our goal here is to provide a complete solution, given arbitrary initial and boundary conditions as dictated by experiment. (Nota bene: In Amblard et al. (1996), Eq. 2 should include a minus sign; as written, the equation is ill-posed.)

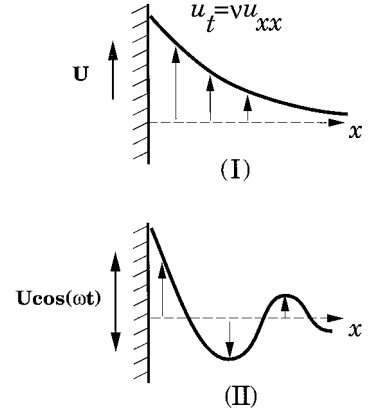

FIGURE 1 Geometry of Stokes problems I and II.

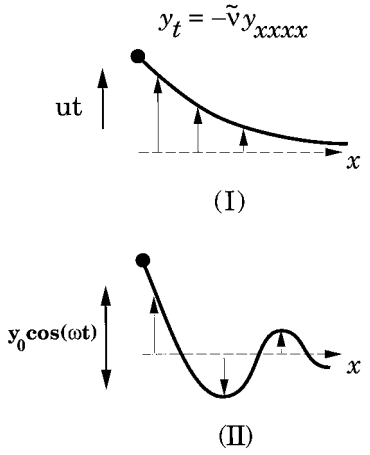

FIGURE 2 Geometry of elastohydrodynamic problems I and II.

An analysis similar to that presented below of the oscillatory passive elastica was carried out a number of years ago by K. E. Machin (Machin, 1958, 1962), who considered the motion of a driven flagellum. Machin was interested specifically in a semiinfinite active flagellum that was bent with a set of boundary conditions amenable to analysis. Ours will be more malicious, but not subtle.

We first recall some general features of equations of motion for elastica embedded in viscous flow. By illustrating the geometrically exact equation, we hope to make clear how higher order terms will affect the results of linearized analysis. We then apply this dynamic to a number of experimentally relevant scenarios. Inspired by Stokes problems I and II in fluid dynamics (SI and SII), we first solve problems I and II of elastohydrodynamics (EHDI and EHDII), each of whose dynamic mimics its hydrodynamic analog. Problem I requires some mathematical details familiar from elasticity theory to assist our physical intuitions. Specifically, we use a set of basis functions appropriate to the equation of motion and specified boundary conditions. All of the pleasant features found when applying Fourier space to unbounded or periodic systems are found here as well, in what we term $\mathcal{W}$-space. Unlike Fourier space, $\mathcal{W}$-space respects both the compact support and the boundary conditions of the elastica and thus diagonalizes the equation of motion. We then discuss an experimental realization of problem II and its analysis, which provides a new technique for the measurement of a polymer's bending modulus. Finally, we comment on experiments by a separate group to which the EHDI analysis may be applied.

ELASTIC FORCES

A bent elastic polymer exerts a restorative force per unit length given by the functional derivative $\mathbf{f}_{\mathscr{E}} = -\delta\mathscr{E}/\delta\mathbf{r}$ of a bending energy,

$$\mathscr{E} = \frac{1}{2} A \int_0^L ds\kappa^2 \tag{3}$$

(Note that we may also include any forces of constraint, such as a Lagrangian tension to enforce inextensibility (Goldstein and Langer, 1995), but such terms will be of higher order in the curvature than we will consider in this investigation.) Here κ is the curvature, s is the arclength, and A is the bending stiffness constant, with units of energy $\times$ length. This may also be expressed as the product EI of Young's modulus E and the moment of inertia I (Love, 1892). For a polymer of persistence length L_p at absolute temperature T, exploring all configurations in D dimensions, we may also derive by equipartition the equivalence $A = (D - 1)k_B T L_p/2$.

Henceforth we consider elastic filaments lying in the plane, the geometry best suited to data acquisition via microscopy. The curvature κ may then be expressed exactly as $d\theta/ds$, where θ is the angle between the tangent to the curve and some fixed axis (see Fig. 3), or equivalently as $\kappa = y_{xx}/(1 + y_x^2)^{3/2}$. Taking the functional derivative of the energy (Eq. 3), we find the force per unit length, exerted purely in the normal ($\hat{\mathbf{n}}$) direction,

$$\mathbf{f}_{\mathscr{E}} = A\left(\kappa_{ss} + \frac{1}{2}\kappa^3\right)\hat{\mathbf{n}} \tag{4}$$

and the boundary conditions $\kappa = \kappa_s = 0$, indicating torquelessness and forcelessness at free ends of elastica (Weinstock, 1974; Landau and Lifshitz, 1986). At hinged or clamped ends different boundary conditions hold, as will be discussed below.

For small deviations from a horizontal line ($|y_x| \ll 1$), $\hat{\mathbf{t}} \simeq \hat{\mathbf{e}}_x$, $\hat{\mathbf{n}} \simeq -\hat{\mathbf{e}}_y$, and the linearized force is

$$\mathbf{f}_{\mathscr{E}} \simeq -Ay_{xxxx}\hat{\mathbf{e}}_y + \mathbb{O}(y_x^2) \tag{5}$$

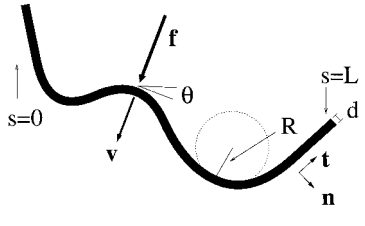

FIGURE 3 Geometry of an elastic filament. R = local radius of curvature = $1/\kappa$; $\mathbf{t}$, $\mathbf{n}$ = unit tangent and normal, $\cos\theta = \hat{\mathbf{t}} \cdot \hat{\mathbf{e}}_x$; d = diameter of the filament; arclength s varies from 0 to L, the total arclength. Within the approximations of slender-body hydrodynamics, a local anisotropic proportionality is satisfied between an external force per unit length $\mathbf{f}$ and the velocity $\mathbf{v}$.

(where $\hat{\mathbf{e}}_y$ is the unit vector in the y direction), with boundary conditions

$$y_{xx} = 0 \quad \text{and} \quad y_{xxx} = 0 \quad \text{at free ends.} \tag{6}$$

The specification of the filament dynamic is complete upon definition of the hydrodynamic drag, which balances $\mathbf{f}_{\mathscr{E}}$. We now turn to this problem.

SLENDER-BODY HYDRODYNAMICS

We consider experiments taking place on cellular biological scales, with typical lengths L in microns, times t in seconds, and a dynamic viscosity μ that of water, in centipoise. The Reynolds number is $UL/\nu \approx L^2/t\nu \approx 10^{-8}/10^{-2} \approx 10^{-6}$, so we are safely in the low-Reynolds number or Stokesian regime. In this Aristotelian overdamped limit, forces balance velocities rather than accelerations. For a body whose length is much greater than its width, the well-developed set of calculations known as slender-body hydrodynamics applies (Keller and Rubinow, 1976; Cox, 1970, 1971). If this filamentous polymer has diameter d, length L, and an aspect ratio $d/L \ll 1$, we have to lowest order in $1/\ln(L/d)$ the simplified, local, anisotropic proportionality between the drag force $\mathbf{f}_d$ and the velocity $\mathbf{r}_t$,

$$\mathbf{f}_d = \zeta[\hat{\mathbf{n}}\hat{\mathbf{n}} + \beta\hat{\hat{\mathbf{t}}}\hat{\mathbf{t}}] \cdot (\mathbf{r}_t - \mathbf{u}) \tag{7}$$

Here $\mathbf{f}_d(s)$ is a force per unit length exerted on the filament, and $\hat{\mathbf{n}}(s)$ and $\hat{\mathbf{t}}(s)$ are unit vectors in the normal and tangential directions at arclength s along the polymer. The products $\hat{\mathbf{n}}\hat{\mathbf{n}}$ and $\hat{\hat{\mathbf{t}}}\hat{\mathbf{t}}$ indicate tensor multiplication, projecting velocities normal and tangential to the curve and relating them via their respective drag coefficients to the applied force. The velocity of the polymer is denoted $\mathbf{r}_t(s)$, and $\mathbf{u}$ is any background velocity that may be present in the problem; the drag should be a function of the former relative to the latter. The anisotropy, evident when dragging a pencil through molasses, between motions parallel and perpendicular to a slender object's long axis is embodied by the parameter β, which depends logarithmically on the aspect ratio, with asymptotic behavior $\beta \to 1/2$ as $L/d \to \infty$. For small d/L, the viscous drag coefficient ζ has the limiting behavior

$$\zeta = \frac{4\pi\mu}{\ln(L/d) + c} \tag{8}$$

where c is a constant of order unity, which depends on the shape of the body (Keller and Rubinow, 1976; Cox, 1970, 1971; Lighthill, 1975; Childress, 1981; Shelley and Ueda, 1996).

We now equate the elastic force per unit length with the drag force ($\mathbf{f}_d = \mathbf{f}_{\mathscr{E}}$) to derive the equation of motion:

$$\zeta[\hat{\mathbf{n}}\hat{\mathbf{n}} + \beta\hat{\hat{\mathbf{t}}}\hat{\mathbf{t}}] \cdot (\mathbf{r}_t - \mathbf{u}) = A\left(\kappa_{ss} + \frac{1}{2}\kappa^3\right)\hat{\mathbf{n}} \tag{9}$$

Linearizing the expression for the drag (Eq. 7) for nearly straight polymers and noting that its tangential components are of order y_x^2, the dynamic reduces to

$$\zeta(y_t - u) = -Ay_{xxxx} \tag{10}$$

Here $u \equiv \mathbf{u} \cdot \hat{\mathbf{e}}_y$. In the absence of any background flow we recover Eq. 2. This is the simplest linearized expression of elastohydrodynamics: elastic forces, characterized by a fourth spatial derivative, balance viscous drag. It shares many similarities with the diffusion equation (Eq. 1) and may be thought of as "hyperdiffusion" of displacement in analogy with hyperviscosity.

ELASTOHYDRODYNAMIC PROBLEM I

Now that we have established the equation of motion appropriate to these elastohydrodynamic analogs, we recall the solutions to the fluid dynamics problems SI and SII in hopes of exploiting the analogy as much as possible. In Stokes I (SI), a semiinfinite plane of fluid is driven by a wall that is motionless for time $t < 0$ and has velocity $U\hat{\mathbf{e}}_y$ for $t > 0$. In Stokes II (SII), the wall oscillates as $U\cos(\omega t)\hat{\mathbf{e}}_y$, and we solve for the behavior after transients have died away.

As illustrated in Fig. 1, velocity gradients are in the x direction in both Stokes problems, and hence are perpendicular to the direction of flow (along the y axis). In the absence of an imposed pressure gradient, the Navier-Stokes equation for the fluid velocity $u(x, t)$ parallel to the wall is simply the linear diffusion equation (Eq. 1), $u_t = \nu u_{xx}$.

A convenient method of solving SI with the associated boundary condition is to postulate a scaling solution inspired by dimensional analysis: $u(x, t) = UF(\xi)$, with $\xi \equiv x/(\nu t)^{1/2}$. The scaling function F then obeys a nonautonomous ordinary differential equation $-\frac{1}{2}\xi F_\xi = F_{\xi\xi}$, the solution of which is $F = \text{erfc}\,(\xi/\sqrt{2})$, where erfc is the complementary error function. Rewriting Eq. 1 in this form illustrates the scaling behavior alluded to after Eq. 1.

Armed with some understanding of SI, we now turn to problem I of elastohydrodynamics (EHDI). In problem I, we consider an elastic filamentous polymer that is anchored at the origin. For $t < 0$ it lies along the line segment $\{y = 0; 0 < x < L\}$. We then may consider forcing the filament by moving one end relative to the fluid (moving the anchor) or moving the fluid relative to the polymer (moving, for example, the coverslip). We will first attempt to do this in a way as analogous to SI as possible.

The strict analog of SI involves a polymer of infinite extent, obviating the problem of boundary conditions at the "right" end. Although this scenario is of limited value in comparing to experiments on actin or microtubules, where thermal fluctuations dominate on scales longer than the persistence length, it is useful both in illustration of how Eqs. 1 and 2 differ, and in application to more rigid biofilaments, e.g., filaments of *B. subtilis*, whose persistence length is ~10 m (Pederson and Goldstein, unpublished data).

Defining $\xi \equiv x/(\tilde{\nu}t)^{1/4}$, the scaling ansatz $y = utF(\xi)$ transforms Eq. 2 into $F - \frac{1}{4}\xi F_\xi = -F_{\xi\xi\xi\xi}$. Demanding that $F(\infty) \to 0$, we find that the slope $y_x = utF_\xi/(\tilde{\nu}t)^{1/4}$ grows in time without bound, thus failing to meet the criterion on which the linearization of Eq. 9 was predicated: $|y_x| \ll 1$. We therefore turn instead to the case of the finite elastica, clamped at one end and free at the other, and subject to impulsive hydrodynamic drag. Our analysis is applicable to experiments in which either the coverslip is moved or, as a special case, in which the elastica is allowed to relax from some initial condition in the absence of flow.

To make the mathematics as transparent as possible, we first nondimensionalize the equation of motion (Eq. 10). Distances in x are rescaled by the total length L, time by the elastohydrodynamic time scale $\zeta L^4/A$, and distances in y by the (constant) velocity u times this time scale:

$$x = \alpha L, \quad t = \tau\frac{\zeta L^4}{A}, \quad y(x, t) = u\frac{\zeta L^4}{A}h(\alpha, \tau) \tag{11}$$

The governing equation, $y_t - u = -\tilde{\nu}y_{xxxx}$, then becomes

$$h_\tau - 1 = -h_{\alpha\alpha\alpha\alpha} \tag{12}$$

The homogeneous equation is $g_\tau = -g_{\alpha\alpha\alpha\alpha}$. Well versed in the litany of Fourier transforms, we first left-multiply by an as yet arbitrary function $\mathcal{W}_k(\alpha)$ (where k indicates a parameter rather than a derivative) and integrate over the domain of α,

$$\int_0^1 d\alpha \mathcal{W}_k \partial_\tau g = -\int_0^1 d\alpha \mathcal{W}_k \partial_\alpha^4 g \tag{13}$$

Integration by parts of the fourth-order derivative introduces eight separate surface terms. The boundary conditions implied by the functional derivative dictate the vanishing of the second and third derivatives at the free end ($x = L$). Requiring g to satisfy these conditions eliminates two of the eight terms.

The left end of the polymer is clamped at the origin, so $y(x = 0) = y_x(x = 0) = 0$. Demanding this behavior of g eliminates two additional surface terms. We now choose $\mathcal{W}_k$ to satisfy the same boundary conditions as y, g, and h: $\mathcal{W}_k(0) = \partial_\alpha \mathcal{W}_k(0) = \partial_\alpha^2 \mathcal{W}_k(1) = \partial_\alpha^3 \mathcal{W}_k(1) = 0$. This annihilates the remaining four surface terms. Finally, we choose $\mathcal{W}_k$ to obey

$$\partial_\alpha^4 \mathcal{W}_k = k^4 \mathcal{W}_k \tag{14}$$

Defining $g_k \equiv \int_0^1 d\alpha \mathcal{W}_k g$, the equation of motion becomes $\partial_\tau g_k = -k^4 g_k$, the solution to which is

$$g_k(\tau) = g_k(0)e^{-k^4\tau} \tag{15}$$

If we wish to describe the dynamics in such terms, we must construct the $\mathcal{W}_k$, which necessitates that we identify the allowed values of k.

A moment's thought reveals that the $\mathcal{W}_k$ cannot simply be constructed out of the familiar sin's and cos's of Fourier

space, which are incompatible with boundary conditions in which successive derivatives vanish. A countably infinite family of such $\mathcal{W}_k$ can, however, be constructed by including hyperbolic trigonometric functions as well in the basis of the function space. The general solution of Eq. 14 is (Landau and Lifshitz, 1986)

$$\mathcal{W}_k = a_1\sin(k\alpha) + a_2\cos(k\alpha) + a_3\sinh(k\alpha) + a_4\cosh(k\alpha) \tag{16}$$

The expression has four unknowns, as a solution to a fourth-order problem must. Inserting the four boundary conditions leads to a solvability condition for k:

$$\cos k = -\frac{1}{\cosh k} \tag{17}$$

This transcendental equation has an infinite number of solutions. For large values of k, as $1/\cosh k \to 0$, the solutions approach the solutions of the Fourier-like solvability condition $\cos k = 0$, i.e., $k_{n+1} \to \pi/2 + \pi n$. The first few solutions are

$$\begin{aligned} k_1 &\simeq \frac{\pi}{2} + 0.304 \simeq 1.875, \\ k_2 &\simeq \frac{3\pi}{2} - 0.018 \simeq 4.694, \\ k_3 &\simeq \frac{5\pi}{2} + 0.001 \simeq 7.855, \\ k_4 &\simeq \frac{7\pi}{2} \simeq 10.996, \ldots \end{aligned} \tag{18}$$

The first three normalized eigenfunctions are shown in Fig. 4.

Note that had we chosen other boundary conditions, a different solvability condition and eigenfamily would have resulted (cf. Appendix B). For example, in the case of the elastica with free ends, we employ an expansion of y with the basis functions of Eq. B2.

With appropriate boundary conditions, the operator ∂_α^4 can be proved to be self-adjoint, and thus the eigenfunctions constitute a complete basis in function space onto which we may project initial data and relate to later-time solutions via Eq. 15 in the standard Green's function way:

$$g(\alpha, \tau) = \int_0^1 d\alpha' \mathcal{G}(\alpha, \alpha'; \tau) g(\alpha', 0) \tag{19}$$

where the Green's function is

$$\mathcal{G}(\alpha, \alpha'; \tau) = \sum_k \mathcal{W}_k(\alpha)\mathcal{W}_k(\alpha') e^{-k^4\tau} \tag{20}$$

This is the exact solution of the linearized homogeneous equation. Note that the compact support and the boundary conditions break translation invariance, reflected in the fact that $\mathcal{G}$ cannot be expressed as $\mathcal{G}(\alpha - \alpha'; \tau)$.

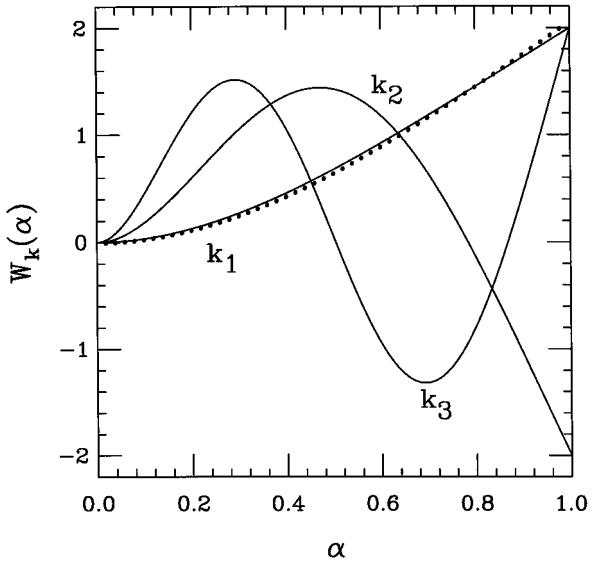

FIGURE 4 The first three eigenfunctions for EHD problem I. The dotted line indicates the normalized third-order polynomial describing an elastica bent by a point force at the right end. Note the surprising overlap with $\mathcal{W}_{k_1}$, as exploited in the text (The Simple EHDI Experiment).

We note from the solution (Eq. 20) that each mode g_k decays independently and exponentially with time. This is to be compared with diffusive problems, in which each mode decays exponentially in time, except for the zero (average) mode, which is constant. In this experiment, the boundary conditions are incompatible with the existence of a zero mode. The system "hyperdiffuses" to homogeneity.

Because $g(\alpha, \tau)$ decays to zero, we have $h(\alpha, \tau) \to \bar{h}(\alpha)$ as $\tau \to \infty$, where

$$\bar{h}(\alpha) \equiv \frac{1}{24}(\alpha^4 - 4\alpha^3 + 6\alpha^2) \tag{21}$$

Returning to the clamped polymer in the presence of some background flow, we project the definitional statement $h(\alpha, \tau) = g(\alpha, \tau) + \bar{h}(\alpha)$ onto the $\mathcal{W}_k(\alpha)$:

$$h_k(\tau) = g_k(\tau) + \bar{h}_k \tag{22}$$

which implies the initial condition $g_k(0) = h_k(0) - \bar{h}_k$. Recalling the simple time dependence of the modes g_k from Eq. 15, we see

$$h_k(\tau) = \bar{h}_k(1 - e^{-k^4\tau}) + h_k(0)e^{-k^4\tau} \tag{23}$$

The dynamic thus mimics that of a capacitor, charging up with the final shape state and draining of the initial shape state, each mode governed independently by decay rate k^{-4}. In the experiment considered, the initial condition is a flat polymer: $h(\alpha, \tau = 0) = 0$. Because $\bar{h}$ is the solution to $\bar{h}_{\alpha\alpha\alpha\alpha} = 1$, with boundary conditions $\bar{h}(0) = \bar{h}_\alpha(0) = \bar{h}_{\alpha\alpha}(1) = \bar{h}_{\alpha\alpha\alpha}(1) = 0$, we find upon integrating by parts

that $\bar{h}_k = k^{-4}\mathcal{W}_k$, where $\mathcal{W}_k \equiv \int_0^1 d\alpha \mathcal{W}_k$, $\bar{h}_k \equiv \int d\alpha \mathcal{W}_k \bar{h}$, and thus

$$h(\alpha, \tau) = \bar{h}(\alpha) - \sum_{k=k_1}^{\infty} \mathcal{W}_k(\alpha) \frac{\mathcal{W}_k}{k^4} e^{-k^4\tau} \tag{24}$$

Evaluating the first few integrals, we find for $\bar{h}_k$, $\bar{h}_{k_1} \simeq 6 \times 10^{-2}$, $\bar{h}_{k_2} \simeq 9 \times 10^{-4}$, $\bar{h}_{k_3} \simeq 7 \times 10^{-5}$, $\bar{h}_{k_4} \simeq 1 \times 10^{-5}$.... Each mode with $k > k_1$ decays exponentially faster in time than the lowest mode, which thus dominates as $\tau \to \infty$, so

$$h \to \bar{h} - \bar{h}_{k_1} e^{-k_1^4\tau} \simeq \bar{h} - 0.06\mathcal{W}_{k_1} e^{-12.36\tau} \tag{25}$$

Our picture of the impulsive dynamic of elastica in viscous flow is thus as follows: we project onto a special function space in which the long-time solution and the difference between initial data and the long-time solution exponentially charge and decay, respectively, each mode behaving independently. We are left with only the long-time solution as the asymptotic limit $\tau \to \infty$.

ELASTOHYDRODYNAMIC PROBLEM II

In Stokes II, the driving force is exerted by a wall oscillating with velocity $\mathbf{u} = U\hat{\mathbf{e}}_y \cos(\omega t)$, or position $y = y_0 \cos(\omega t)$. To solve the steady-state limit of SII, we postulate $u(x, t) = U\Re(e^{i\omega t}G(\eta))$, where $\eta = x(\omega/\nu)^{1/2}$ and $\Re(z)$ indicates the real part of z. Inserting into Eq. 1, we then see that G satisfies

$$iG = G_{\eta\eta} \tag{26}$$

for which the solution vanishing as $\eta \to \infty$ is $G = e^{-\sqrt{i}\eta}$. We then find that $u(x, t) = Ue^{-\eta/\sqrt{2}} \cos(\omega t - \eta/\sqrt{2})$, or, in a form useful for comparison to the elastohydrodynamic case,

$$u(x, t) = Ue^{-S\eta}\cos(C\eta - \omega t) \tag{27}$$

where $C = \cos(\pi/4)$ and $S = \sin(\pi/4)$. This solution describes right-moving waves of velocity $\omega\ell_S/C$, decaying as $x \to \infty$ with decay length ℓ_S/S.

We now consider a polymer held by an optical trap that moves with position $y(x = 0) = y_0 \cos(\omega t)$. Because we have shown in the previous section that all modes satisfying the homogeneous equation of motion with homogeneous boundary conditions decay exponentially, we must only find a solution in the presence of inhomogeneity (here, the driving) to find the long-time limit of the dynamic.

To verify the validity of our analysis as well as the plausibility of EHDII as a method for measuring biopolymer rigidity, we conducted the experiment (Riveline et al., 1997) and analyzed image data as described below. A scaling relation predicted by the analysis was confirmed, and a new method for measurement of the persistence length of actin was demonstrated.

The experimental setup is shown in Fig. 5: F-actin is bound to a latex bead, which is optically trapped. As the position of the bead oscillates sinusoidally in time, the filament wiggles back and forth, propagating waves of displacement down its length. The motion relative to the fluid is opposed by the fluid viscosity, and the "wiggles" are opposed by the elasticity of the polymer.

The elastic constant A has units of energy $\times$ length, and the viscous force per unit length per unit velocity has the dimensions of a viscosity or action density μ:

$$[\zeta] = [\mu] = \frac{\text{mass}}{\text{length} \times \text{time}} = \frac{\text{energy} \times \text{time}}{\text{length}^3} \tag{28}$$

Thus the natural length obtained from A, ζ, and the frequency of oscillation ω is

$$\ell(\omega) = \left(\frac{A}{\omega\zeta}\right)^{1/4} = \left(\frac{k_B T L_p}{\omega\zeta}\right)^{1/4} \tag{29}$$

Nota bene that $\ell(\omega)$ is not a mere rescaling of the persistence length.

With a previously published persistence length for actin of $L_p \simeq 15$ μm (Ott et al., 1993), a viscosity $\mu = 0.01$ cp, $k_B T \simeq 4 \times 10^{-14}$ erg at $T = 300$ K, and measuring ω in units of s^{-1}, we obtain

$$\ell(\omega) \simeq \left(2.8 \frac{\mu\text{m}}{s^{1/4}}\right)\omega^{-1/4} \tag{30}$$

Thus for frequencies on the order of 1 Hz, we obtain length scales on the order of microns, somewhat below the persistence length. This range of frequencies seems quite advantageous for experiment.

This elastohydrodynamic length $\ell(\omega)$ is precisely the length found upon nondimensionalizing the equation of motion (Eq. 2). By analogy to SII, we define the dimensionless coordinate $\eta = x/(\tilde{\nu}\omega)^{1/4} = x/\ell(\omega) = x(A/\omega\zeta)^{-1/4}$

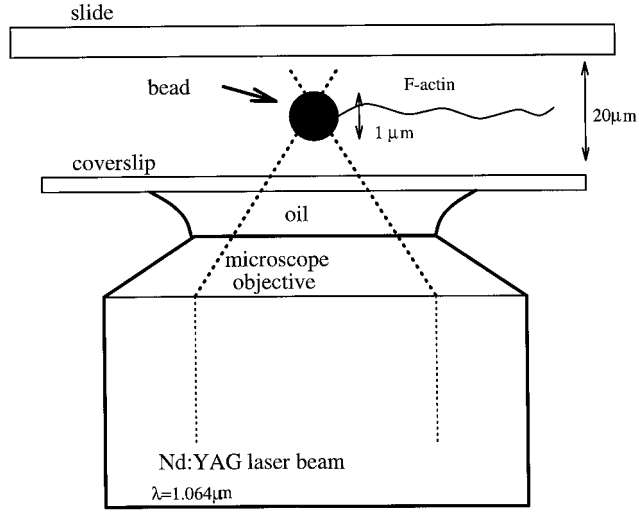

FIGURE 5 Experimental setup.

and rewrite the solution as

$$y(x, t) = y_0 \Re\{e^{i\omega t} h(\eta)\} \tag{31}$$

and Eq. 2 as

$$ih = -h_{\eta\eta\eta\eta} \tag{32}$$

The solutions of Eq. 32 are of the form $h(\eta) = ce^{\gamma\eta}$, where γ may be any one of the four distinct (complex) numbers such that $\gamma^4 = -i$. These are $\gamma_j = i^j \exp(-i\pi/8), j = 1 \ldots 4$. The general solution is the sum of these four solutions,

$$h(\eta) = \sum_{j=1}^{4} c_j e^{i^j z_0 \eta} \tag{33}$$

where $z_0 \equiv e^{-i\pi/8} \simeq 0.92 - 0.38i$. The unpleasant (but certainly not subtle) remainder of the problem is to solve for the four c_j's, given some four boundary conditions. At the left ($x = 0$) end, we enforce the position and the condition of torquelessness (as appropriate for an optical trap): $y_{xx}(0) = 0$. The right end must satisfy the free end boundary conditions (Eq. 6). The c_j derived from these conditions are functions of a rescaled polymer length $\mathcal{L} \equiv L/\ell(\omega)$ and may properly be written as $c_j(\mathcal{L})$.

Semiinfinite polymer

The exact solution for $h(\eta)$ is presented in Appendix C; it simplifies greatly, however, for extreme values of $L/\ell(\omega)$. For this reason we include a discussion of the polymer of infinite extent. In this limit, the two coefficients c_j for which γ_j has a nonnegative real part must be zero, allowing only decaying solutions as $x \to \infty$.

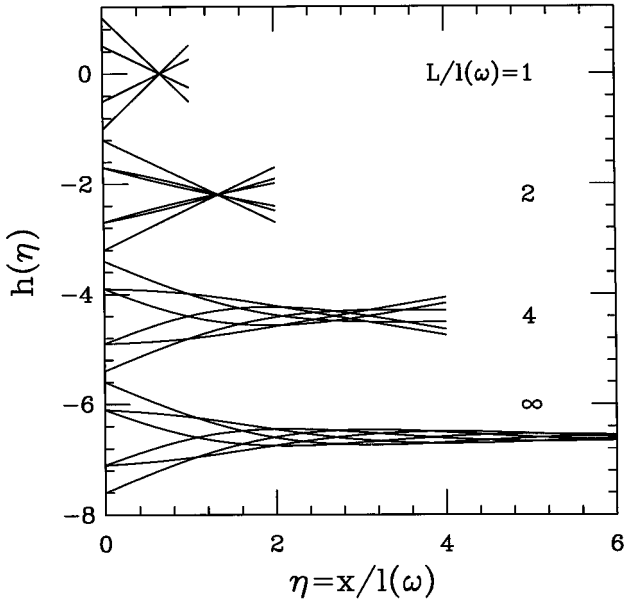

FIGURE 6 Solutions to EHD problem II for filaments of various rescaled lengths $\mathcal{L}$.

The solution consistent with the two left-end boundary conditions is

$$y = \frac{y_0}{2}\left[e^{-\tilde{C}\eta}\cos(\tilde{S}\eta + \omega t) + e^{-\tilde{S}\eta}\cos(\tilde{C}\eta - \omega t)\right] \tag{34}$$

where $\tilde{C} = \cos(\pi/8)$ and $\tilde{S} = \sin(\pi/8)$. Compare with the solution to SII (Eq. 27). The semiinfinite solution (Eq. 34) is shown at the bottom of Fig. 6 for $\omega t = n2\pi/6$, $n = 1 \ldots 6$. In the hydrodynamic case, the solution of Eq. 27 describes exponentially decaying right-moving traveling waves of transverse velocity. In the elastohydrodynamic case, the higher order derivative allows more complicated behavior: right- and left-moving waves of displacement, with different decay rates and velocities. In this case, the right-movers have a slower decay (because $\tilde{S} \simeq 0.38 < 0.92 \simeq \tilde{C}$), and might be expected in some sense to dominate over the left-movers. This mechanism will be elaborated on below (under Propulsive Force).

Finite polymer

In the limit of a short or stiff polymer, $\mathcal{L} \ll 1$, we rewrite $\eta = \alpha\mathcal{L}$, $\alpha = x/L \in (0, 1)$ and expand, yielding

$$h < (\alpha) \simeq \left(1 - \frac{3}{2}\alpha\right) + \frac{i\alpha\mathcal{L}^4}{1680}(-16 + 70\alpha^2 - 70\alpha^3 + 21\alpha^4) \tag{35}$$

Equivalently, we may derive this polynomial by truncating a series expansion for h in α and enforcing the equation of motion (Eq. 32) and the boundary conditions (Eq. 6). Using Eq. 35, all four boundary conditions are satisfied exactly, whereas Eq. 32 is solved to order $\mathcal{O}(\mathcal{L}^4)$.

The exact solution is shown in Fig. 6 for $\mathcal{L} = 1, 2, 4$, and ∞ and $\omega t = n2\pi/6$, $n = 1 \ldots 6$. Note the existence of a pivot point at $x = 2L/3$ as $\mathcal{L} \to 0$. This behavior is described by the $\mathcal{O}(\mathcal{L}^0)$ term in Eq. 35: as $\mathcal{L} \to 0$, the polymer acts as a rigid rod. As a consequence, it is impossible to tell if a movie of such a polymer is being played forward or backward. Indeed, this is a filamentous version of the famous "one-armed swimmer" or "scallop" example, illustrating the lack of net propulsion for rigid objects executing time-reversible motions in low Reynolds number flow (Purcell, 1977; Childress, 1981).

Propulsive force

Problem II and its associated experiment are sufficiently reminiscent of flagellar hydrodynamics to motivate a calculation of the propulsive force F generated in the x direction by the wiggling. This can be done by integrating $\mathbf{f}_{\mathcal{L}}$, the force exerted by the polymer on the fluid, along the length of the filament. We then contract this instantaneous total force with $\hat{\mathbf{e}}_x$ and average over one period. This force is

equal to and opposite the propulsive force exerted by the fluid on the polymer.

Noting that the force per unit length in Eq. 4 is a total derivative,

$$\mathbf{f}_{\mathscr{E}} = A\partial_s\left(\kappa_s\hat{\mathbf{n}} - \frac{1}{2}\kappa^2\hat{\mathbf{t}}\right) \tag{36}$$

and recalling the boundary conditions imposed on κ and κ_s, we have

$$F \equiv -\int \mathrm{d}s\mathbf{f}_{\mathscr{E}}\cdot\hat{\mathbf{e}}_x = A\kappa_s\sin\theta(s=0) \tag{37}$$

This is geometrically exact. We now wish to calculate the time average $\bar{F}$ over one period. Within the linearized solution, $\kappa_s \sin\theta \simeq y_{xxx}y_x$. Recalling the expression for y in Eq. 31, we obtain

$$\bar{F} = \frac{y_0^2\zeta\omega}{4\sqrt{2}}\Upsilon\left(\frac{L}{\ell(\omega)}\right) \tag{38}$$

where $\ell(\omega)$ is the characteristic length and Υ is a scaling function conveniently normalized (see below).

The exact solution to EHDII given in Appendix C can be used to calculate the function Υ for all values of the polymer length. The asymptotic behavior as $\mathscr{L} \to \infty$ is

$$\Upsilon(\mathscr{L}) \to 1 + 4e^{-2\tilde{S}\mathscr{L}}\sin(2\tilde{C}\mathscr{L}) \tag{39}$$

When the length is short compared to the characteristic length, the polymer flexes very little, so

$$\Upsilon \simeq \frac{11}{3360}\mathscr{L}^4 + \mathcal{O}(\mathscr{L}^8) \simeq \frac{11}{3360}\frac{\zeta\omega}{A}L^4 \tag{40}$$

As Fig. 7 illustrates, the short-length approximation (Eq. 40) shows good agreement with the exact solution for $\mathscr{L} \lesssim 3$, as does the large-$\mathscr{L}$ approximation (Eq. 39) for $\mathscr{L} \gtrsim 3$. The approach to the asymptotic limit is oscillatory, with a maximum near $\mathscr{L} \approx 4$, the value at which $\Re\{h_\eta\}$ acquires its first root, and a local minimum near $\mathscr{L} \approx 6$, the value at which $\Im\{h_\eta\}$ acquires its second root. The unexpected local maximum indicates that there is an optimal combination of A, ω, and a finite L.

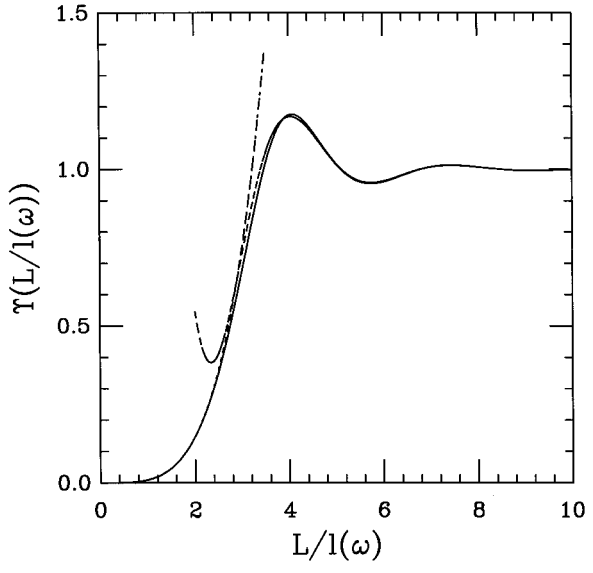

FIGURE 7 Scaling function Υ for propulsive force. The large $\mathscr{L}$ expansion is plotted for $\mathscr{L} > 2$, and the small-$\mathscr{L}$ solution is plotted for $\mathscr{L} < 3.5$.

Inserting typical numbers from the experiment (in cgs),

$$\mu \approx 10^{-2}, \quad y_0 \approx 4\times10^{-4}$$

$$\omega \approx 2\pi, \quad \frac{L}{d} \approx 10^3$$

we find that $F(\infty) \approx 2\times10^{-9}$ dynes $= 3\times10^{-2}$ pN. For a trap stiffness of ~0.02 pN/nm, this would induce a displacement of 1.5 nm, at the lower limit of experimental observation. The production and measurement of propulsive force by an artificial flagellum were attempted by G. I. Taylor (Taylor, 1952), using a glycerine-filled tub to mimic the low Reynolds numbers found in vivo. Taylor struggled to drive the flagellum without inducing unwanted torque or disturbing the flow, a difficulty obviated by the use of optical traps.

Returning to the asymptotic expressions for h derived in the previous two sections, we observe a pleasant accordance with the qualitative features of Fig. 7. In the semiinfinite case, we noted the presence of right- and left-movers, with right-moving waves of displacement exhibiting slower decay. Such a dominance accounts for the nonzero propulsive force in the $\mathscr{L} \to \infty$ limit, where a net propulsion to the left survives. In the $\mathscr{L} \to 0$ case, we recovered a shape that approaches a pivoting rigid rod, not unlike a one-armed swimmer. As we expect from life at low Reynolds number (Purcell, 1977; Childress, 1981), such a motion, invariant under $t \to -t$, can produce no net propulsion.

As a further illustration of the relationship between low-Reynolds-number swimming and cyclic motions, we observe that the lowest-order expression for the time-averaged force is equal to

$$F = \frac{\zeta\omega}{2\pi}\int_0^{2\pi/\omega}\mathrm{d}t\, y_x\Big|_{x=0}\frac{\mathrm{d}}{\mathrm{d}t}\int_0^L \mathrm{d}x\, y(x) \tag{41}$$

or, noting that $\int_0^L \mathrm{d}x\, y(x,t)$ is simply the area $\mathscr{A}(t)$ under the curve $y(x,t)$, and that the slope at the left is to first order simply the tangent angle θ_0,

$$F = \frac{\zeta\omega}{2\pi}\int_0^{2\pi/\omega}\mathrm{d}t\,\theta_0\frac{\mathrm{d}\mathscr{A}}{\mathrm{d}t} = \frac{\zeta\omega}{2\pi}\oint\theta_0\,\mathrm{d}\mathscr{A} \tag{42}$$

This result can be interpreted quite simply: the propulsive force results from pushing aside some volume (or in two dimensions, an area) of fluid, projected in the direction of propulsion $\hat{\mathbf{e}}_x$ an amount proportional to θ_0. Note that had we been interested in the propulsion in the transverse ($\hat{\mathbf{e}}_y$)

direction, the θ_0 would not appear, leaving the absence of net forcing: $F \propto \oint d\mathcal{A} = 0$, as we would expect.

The net force, then, is the area enclosed by a trajectory in $\mathcal{A} - \theta_0$ space during some cyclic motion. This representation is independent of the particular motion exhibited, although we have here considered simple periodic motion, for which the trajectory is always an ellipse. As $\mathcal{L} \to 0$, the elliptical trajectory thins to a straight line, encloses no area, and thus produces no force.

This representation makes clear that in an inertialess world, net motion is principally geometric in origin rather than dynamic (Shapere and Wilczek, 1987). In a manner analogous to the importance of path rather than kinetics in generating net work in a Carnot diagram, we see that we can remove time entirely from the expression and consider instead a path in a low-dimensional projection of the infinite-dimensional shape space.

ANALYSIS OF EXPERIMENTS

Actin

As mentioned in the previous section, the EHDII experiment was performed and the data compared to the solution of Eq. 32. In this way we were able to confirm the results of the analysis and investigate a new method for measuring biopolymer bending moduli. Materials used in the experiment may be found in Riveline et al. (1997).

Knowing the amplitude of the driving of the bead (y_0) and the frequency (ω), and reading off the projected length (L) and the phase (ωt) directly from the images, we are left with a one-parameter fit of the images to the solution of Eq. 32, varying only $\ell(\omega)$ to minimize χ^2. We can then observe the dependence of ℓ on ω, as illustrated in Fig. 8. The variation in error bars can be attributed to the widely varying number of images taken at different frequencies.

Comparing with the earlier analysis (cf. the previous section), we can extract from this scaling a measurement of the persistence length. Fitting to

$$\ell(\omega) = \left(\frac{k_B T}{\zeta}\right)^{1/4} L_p^{1/4} \omega^{-1/4} \tag{43}$$

we determine L_p to be 7.4 ± 0.2 μm.

There are a few limitations with this realization of the experiment which, upon correction, will improve this technique and make the data more conclusive. An obvious mechanism for improving the error bars is to accumulate more data. Image-taking was entirely manual; automation of this process would clearly be advantageous and improve the low statistics used here. Furthermore, with careful control of the timing, images of equal phase can be superposed to average out thermal fluctuations or experimental variation in the images before fits are performed.

Most importantly, because our aim was to verify the plausibility of the experiment, we did not limit ourselves to small-amplitude wiggling, thus leaving the realm of validity of the small-y_x approximation. We can estimate the error due to such driving by looking at the relevant terms from the geometrically exact equation of motion:

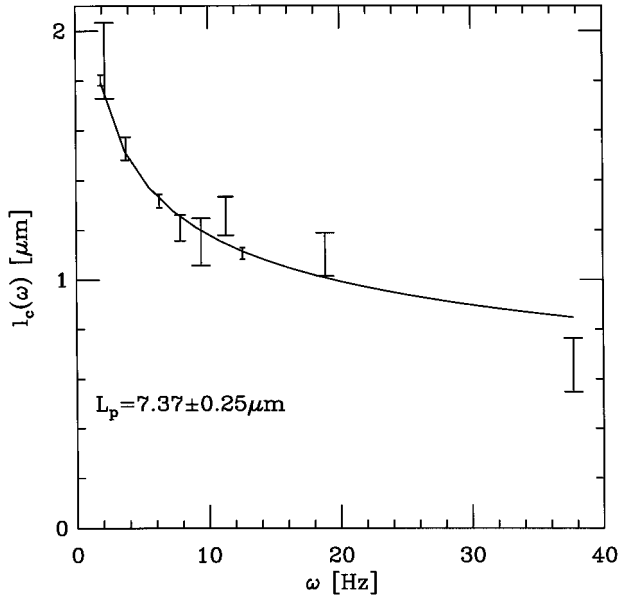

FIGURE 8 The characteristic length scale $\ell(\omega)$ versus frequency ω. The smooth curve is a fit to Eq. 41 for L_p = 7.4 μm. The scaling of the characteristic length with the fourth root of time suggests that actin is well described by Eq. 2 and is thus a semiflexible polymer, with a scale-independent elasticity.

$$\frac{y_t}{(1 + y_x^2)^{1/2}} = -\tilde{\nu}\left(\frac{y_{xx}}{(1 + y_x^2)^{3/2}}\right)_{ss} \tag{44}$$

If we wish to approximate this with Eq. 7, we are measuring an "effective" $\tilde{\nu}$ (or "$\tilde{\nu}$") where

$$\text{“}\tilde{\nu}\text{”} \simeq \frac{\tilde{\nu}}{\langle (1 + y_x^2)^2 \rangle} \tag{45}$$

where the brackets indicate averaging over the data, and thus the true A will be underestimated by a factor of $\langle (1 + y_x^2)^2 \rangle$, which is always greater than unity. Inspecting Fig. 9, we see that there are data for which y_x is not necessarily small. For this reason, the data we collected can only put a lower bound on A. We anticipate that the true value may be greater by a factor of up to ~1.5; clearly, future experiments should employ smaller amplitude driving.

We also anticipate that a more accurate treatment of the geometry and hydrodynamics would refine the technique. The true geometry is nonlinear and the hydrodynamics nonlocal, but neither is intractable and both are amenable to numerics. The geometrically exact, intrinsic formulation involves some enjoyable mathematics of curve dynamics, whereas the linearized treatment presented herein is more illustrative and more easily connected with experiment. Similarly, in an attempt to make the analysis as clear as possible, we have omitted from Eq. 7 the background flow due to the trapped bead.

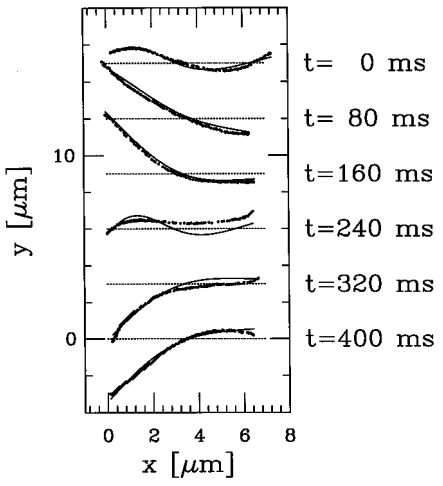

FIGURE 9 Series of typical images of driven actin filaments in EHDII. Also shown are fits to the solution of Eq. 32.

Some amount of discussion has been entertained in the biophysical community about the possible scale or time dependence of the elasticity of biopolymers, including both actin (Käs et al., 1993) and microtubules (Kurachi et al., 1995). One of the more powerful features of this technique is that, because ω and thus $\ell(\omega)$ are controlled by the experimenter, specific scales and frequencies can be investigated to attempt a spectroscopy of elasticity. Equation 4 can be extended without difficulty to include a characteristic plasticity time scale τ or a continuum of times, in an attempt to model a characteristic rate of bond-breaking in the presence of bending. Similarly, one can include additional bending moduli that depend on higher-order derivatives. For oscillatory motion, occurrences of ∂_t are simply replaced by $\partial_t + 1/\tau$ or $i\omega + 1/\tau$. Including higher order derivative terms simply results in replacing Ay_{2x}^2 with $Ay_{2x}^2 + By_{4x}^2$ in the bending energy and Ay_{4x} with $Ay_{4x} + By_{8x}$ in the equations of motion. We then may recover such an equation as

$$\zeta\left(\partial_t + \frac{1}{\tau}\right) y = -Ay_{xxxx} - By_{8x} \tag{46}$$

which can be solved in the manner of Eq. 2. This more general expression makes possible the experimental confirmation or refutation of such hypothesized mechanisms.

Microtubules

A recent pair of elastohydrodynamic experiments involving microtubules (Felgner et al., 1996), brought to our attention as the original version of this paper was being completed, provides an excellent opportunity to apply the spirit of analysis that we have developed for EHDI. In both, the crucial experimental observable is the motion of the free end of a microtubule; the analysis must then relate this motion to the bending modulus A. Experiments were conducted such that the tangent angle, the relevant small parameter, did not exceed 0.1. Hence the linearized treatment outlined for EHDI is appropriate.

We will first investigate the analysis appropriate to a special case of EHDI in which a polymer relaxes to a straight configuration in the absence of a driving flow. We then investigate a more complicated experiment in which an optical trap exerts a point force in the middle of the polymer.

The simple EHDI experiment

In the first experiment (Felgner et al., 1996), a microtubule is initially clamped at the left to an axoneme and trapped directly at the free end; the polymer is bent out of its mechanical equilibrium configuration (cf. Fig. 10 *a*). When the trap is shut off, the polymer relaxes back to the straight shape in a way that we may describe as before: the initial condition is projected onto the appropriate space, in which each mode decays independently.

What remains, then, is merely to determine the initial data: the shape of a biopolymer clamped at one end and held by a trap at the other. For the elastica exerting a bending moment $\mathbf{m}$ under some external force $\mathbf{f}_e$, the (geometrically exact) general equations of force and torque balance for the elastica may be combined into the single equation

$$\mathbf{m}_s = \hat{\mathbf{t}} \times \int_0^s d\sigma\, \mathbf{f}_e(\sigma) \tag{47}$$

where $\hat{\mathbf{t}} = \mathbf{r}_s$ is the unit tangent. In two dimensions, cross products are scalars, and $\mathbf{m}_s$ becomes the scalar m_s.

Using $m = A\theta_s$, and considering point external forces (exerted by the axoneme and the trap) that act at the left and right ends, we rewrite Eq. 47 (for $0 < s < L$) as

$$A\theta_{ss} = -F_y \cos\theta + F_x \sin\theta \tag{48}$$

where $F_{\{x,y\}}$ are the components of the force exerted by the trap, rather than by the axoneme. We expect $F_x < 0$ and F_y

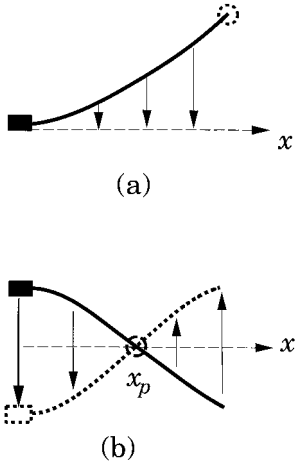

FIGURE 10 EHDI experiments (*a*) A simple special case. (*b*) End-driving as well as driving via a point force.

> 0. Equation 48 is geometrically exact and can be solved in terms of elliptic integrals.

Note that there is no reason to assume the trap exerts a force only in the $\hat{\mathbf{e}}_y$ direction—the oft-quoted "cantilevered beam" problem from introductory civil engineering texts. However, assuming that the polymer is homogeneous along its arclength, there is no energy cost upon moving the trap along the axis of the polymer. Therefore the trap can exert no force in the tangential direction. Accordingly, $F_x/F_y \simeq -dy/dx$, and Eq. 48 linearizes to

$$Ay_{xxx} = -F_y(1 + \mathcal{O}(y_x^2)) \simeq -F_y \tag{49}$$

We now must consider the boundary conditions. The axoneme clamps the left end of the polymer; thus $y(0) = y_x(0) = 0$. Because there is no energy cost to rotating a polymer held in an optical trap, there should be no bending moment, implying that $y_{xx}(L) = 0$. Given these three boundary conditions, the solution to (49) is

$$y(x) = \frac{\tilde{y}}{2}(3\alpha^2 - \alpha^3), \quad \tilde{y} \equiv y(L) = \frac{F_y L^3}{3A} \tag{50}$$

where again, $\alpha \equiv x/L$.

Now that we have our initial data, we project it onto a function space in which the dynamics are simply exponential relaxation. In keeping with the experiment we seek here to model, we focus on the motion of the free end, whose rate of relaxation provides a direct means of measuring the bending modulus A. Given the dramatic increase in relaxation rates for each subsequent mode (cf. Eq. 15), we expect only the lowest mode to be relevant beyond negligible initial times. Moreover, inspecting Fig. 4, we observe that the eigenfunction $\mathcal{W}_{k_1}$ well approximates the normalized third-order polynomial that describes the initial data, whereas higher modes more closely resemble Fourier modes. This close agreement, rather surprising from a sum of trigonometric and hyperbolic trigonometric functions, leads to the dominance of the projection of initial data onto the first mode; specifically, $y_{k_1}(0) \simeq 0.485\tilde{y}$; $y_{k_2}(0) \simeq -0.012\tilde{y}$, where we define $y_{k_n} \equiv \int_0^1 d\alpha\, y\mathcal{W}_{k_n}$, in analogy to Eq. 15. Inserting typical numbers ($A \approx 5 \times 10^{-15}$ dynes cm^2, $L \approx 10 \times 10$ μm, and the drag coefficient from Eq. 8 with $d \approx 20$ nm and $\mu \approx 0.01$ erg s/cm^3), we see that for times beyond 0.01 s, the amplitudes of subsequent modes are, at most, 1% that of the first mode. The shape is then described by $y(x) \simeq \mathcal{W}_{k_1}(x)y_{k_1}(t)$ and decays as e^{-rt}, with $r \equiv Ak_1^4/\zeta L^4$. In the model accompanying the experiment, it was assumed that the shape was described by a single decaying mode for all times beginning at $t = 0$. Fortunately, as we have shown, $\mathcal{W}_{k_1}$ well approximates the initial data such that this introduces only an error $\mathcal{O}(10^{-2})$. Within these approximations, the free end decays as

$$\frac{y(L, t)}{y(L, 0)} \simeq 0.971e^{-rt} \simeq e^{-rt} \tag{51}$$

so that a measurement of the e-folding time yields r and hence A. It is now clear that the identity of k_1, the solution to the transcendental equation (Eq. 17), is crucial, as it is physically manifested in the decay rate.

The model of Felgner et al. (1996) is based first on the computation of the deflection y_l of the free end of the clamped elastica experiencing a flow linearly increasing in x and constant in time, with a drag coefficient $\tilde{\zeta}$. Such a flow would be appropriate for a rigidly rotating rod with constant angular velocity, rather than for the bent elastic filament, for which $y_t(x, t)$ is nonlinear in both variables. Second, to find the decay rate of Felgner et al. (1996), the exponential relaxation of the tip must correspond to some first-order differential equation. Although this equation is not stated, we must assume it to be $y_t(t) = -(v/y_l)y(t)$, (where v is the maximum flow velocity used in the computation of y_l) to recover the reported decay rate,

$$r = \frac{120}{11}\frac{\text{"}A\text{"}}{\tilde{\zeta}L^4} \tag{52}$$

where "A" refers to the value of A that would be extracted from data, using the simplifications described above.

A careful analysis of the drag coefficient in slender-body hydrodynamics employs a matched asymptotics for the fluid velocity and is dependent on the shape of the slender body. Treating a microtubule as a cylinder, the appropriate drag coefficient is (Cox, 1970a)

$$\zeta = \frac{4\pi\mu}{\ln(L/d) + 2\ln 2 - (1/2)} \tag{53}$$

Unfortunately, the drag coefficient used by Felgner et al. (1996) is that appropriate to tangential rather than normal flow, with numerator $2\pi\mu$, and further suffers from the replacement of the constant terms in the denominator of Eq. 53 with $-\ln 2$.

We may now compare the results of a differential equation-motivated analysis with the model of Felgner et al. (1996). Given some measured e-folding time t_*, the eigenmode analysis yields the bending modulus A as

$$A = \frac{\zeta L^4}{t_*}k_1^{-4} \tag{54}$$

whereas the rodlike treatment implies (from Eq. 52)

$$\text{"}A\text{"} = \frac{\tilde{\zeta}L^4}{t_*}\frac{11}{120} \tag{55}$$

Inserting typical numbers from the experiment, $L \approx 10$ μm, $d \approx 0.02$ μm, we see that

$$\frac{\text{"}A\text{"}}{A} = 1.13\frac{\tilde{\zeta}}{\zeta} \simeq 0.709 \tag{56}$$

a systematic underestimate beyond the uncertainties of experiments.

The discontinuous EHDI experiment

A more complicated example of EHDI that was also conducted includes driving the axoneme, so that we must incorporate an inhomogeneous boundary condition, and point forcing by an optical trap (Felgner et al., 1996). In this experiment, the axoneme (attached to the coverslip) is moved with constant velocity v_c between two extreme positions. During this motion, the polymer is constrained by the optical trap to pass through some intermediate point (x_p, y_p). From the position and velocity of the free end, it is possible to determine the bending modulus. Enumerating all of the relevant forces, we consider the force at the left end due to the axoneme, F_a, the point force due to the trap F_p, and the force per unit length due to drag, $-\zeta y_t$ (cf. Fig. 10 *b*). We insert these terms into the equation of force and torque balance for the elastica (Eq. 47) to find the equations of motion.

We adopt an expansion in θ, keeping only the first-order terms. Identifying the external force as the drag, and defining v_c as the constant coverslip velocity, the integrand in Eq. 47 becomes $\zeta\hat{\mathbf{e}}_y(y_t + v_c)$.

Noting, as in Eq. 49, the constraint that the force on a polymer due to an optical trap must have no tangential component, and taking the axoneme to exert a force F_a at $x = 0$ and the trap to exert a point force F_p at $s = s_p$ ($x \simeq x_p$), the y component of the linearized equation reduces to $A\theta_{ss} \simeq F_a - F_p\Theta(s - s_p) - \zeta\int^s ds(y_t + v_c)$, which upon differentiation implies

$$\zeta(y_t + v_c) = -Ay_{xxxx} - F_p\delta(x - x_p) \tag{57}$$

This is our working equation, obtained from the linearized second derivative of the equation of net torquelessness.

Because we do not know the magnitude of F_p a priori, we must perform a matching of $y^a(x)$, the curve describing the anchored end, and $y^f(x)$, the curve describing the free end, which solve

$$\zeta(y_t^{\{a,f\}} + v_c) = -Ay_{xxxx}^{\{a,f\}} \tag{58}$$

subject to matching conditions at the point of forcing. This provides an example of a biopolymer subject both to drag and to micromanipulation via some point force and boundary condition. We will separate the solutions into the homogeneous and the particular, and in a procedure that is now familiar, construct the appropriate function space in which the dynamic is simple.

Inspecting the equation of motion (Eq. 57), we see that it supports a discontinuity in y_{xxx}; however, y_{xx} is continuous, as are y and y_x. Moreover, if we wish to describe an experiment in which the filament position is constrained at the point of forcing x_p, we have not only the matching condition $y^a(x_p) = y^f(x_p)$, but the stronger condition $y^a(x_p) = y^f(x_p) = y_p$; here we choose y_p to be 0 without loss of generality. We thus describe a polymer pinned at a certain intermediate point along the curve by an optical trap, while the right and left sides perform some coupled motion.

At the free end, we impose forcelessness and torquelessness, $y_{xxx}(L) = 0$ and $y_{xx}(L) = 0$, respectively. At the anchored end, the polymer is clamped to the axoneme position $y_A(t)$; thus $y(0) = y_A(t)$, $y_x(0) = 0$. The above-listed boundary conditions constrain four of the arbitrary constants, the remaining matching equations constitute the remaining four, and we may thus completely specify the solution.

The governing equation is linear, allowing us to separate y into two separate solutions of Eq. 58: $y = y_0(h + g)$, where y_0 is some typical length scale. We choose $g(h)$ to satisfy the (in)homogeneous boundary conditions and equation of motion. Compare this with the first example solution of EHDI, in which h was chosen to satisfy an inhomogeneous equation of motion but homogeneous boundary conditions.

As described above, the axoneme moves with constant velocity v_c from $y_A = \Delta$ to $y_A = -\Delta$: $y_A(t) = -v_c t$; $-\Delta/v_c < t < \Delta/v_c$. We must now merely solve for the inhomogeneous solution, expressed as

$$h^{\{a,f\}}(x, t) \equiv \sum_{n=0}^{\infty} c_n^{\{a,f\}}(t)x^n \tag{59}$$

However, we are considering a Stokesian dynamic, in which the time dependence is first-order and the equation of motion is linear; the driving is a constant in time, and thus time should enter only linearly into any steady-state solution for the position (cf. Landau and Lifshitz, 1987). Constraining $\partial_t^2 c_n^{\{a,f\}} = 0$, enforcing the eight matching and boundary conditions, and respecting the relationship between $\partial_t c_n$ and c_{n+4} dictated by Eq. 58, we completely specify the solution. To make explicit the qualitative behavior in limiting cases, and to write the equations as compactly as possible, we employ three nondimensionalized variables:

$$\alpha \equiv \frac{x}{x_p}, \quad \sigma \equiv \frac{x - x_p}{L - x_p}, \quad \tau \equiv t\frac{A}{\zeta x_p^4} \tag{60}$$

The coordinates $\{\alpha, \sigma\} \in (0, 1)$ measure distance on the left from the axoneme and on the right from the trap, and τ is the time rescaled by the characteristic elastohydrodynamic time for the anchored section. The fact that x_p, rather than $l \equiv L - x_p$, appears explicitly in our choice of definition of τ is reflected in the equation of motion, in that the functions now solve slightly different equations for the two sides:

$$\begin{aligned} h_\tau^a + \frac{v_c}{y_0}\frac{\zeta x_p^4}{A} &= -h_{\alpha\alpha\alpha\alpha}^a \\ h_\tau^f + \frac{v_c}{y_0}\frac{\zeta x_p^4}{A} &= -\left(\frac{x_p}{l}\right)^4 h_{\sigma\sigma\sigma\sigma}^f \end{aligned} \tag{61}$$

The natural choice for y_0 is clearly $y_0 = v_c \zeta x_p^4/A$, whereupon we are left with the dimensionless equations of motion,

$$\begin{aligned} h^a_\tau + 1 &= -h^a_{\alpha\alpha\alpha\alpha} \\ h^f_\tau + 1 &= -\rho^4 h^f_{\sigma\sigma\sigma\sigma} \end{aligned} \tag{62}$$

where we have introduced the ratio of lengths

$$\rho \equiv \frac{x_p}{L - x_p} = \frac{x_p}{l} \tag{63}$$

which describes the location of the point of forcing x_p relative to the "extra" length l. As x_p nears the anchored ($x = 0$) end, $\rho \to 0$, and as x_p nears the free ($x = L$) end, $\rho \to \infty$. The solutions to (62) are presented in Appendix D.

As described before, the solution h to the inhomogeneous boundary conditions will describe the long-time behavior remaining after transients decay exponentially. We now turn our attention to the transient g, which must satisfy the homogeneous boundary conditions $g(0) = g_x(0) = g_{xx}(L) = g_{xxx}(L) = g(x_p) = 0$ and matching conditions $[g_x(x_p)] = [g_{xx}(x_p)] = 0$, where the brackets indicate discontinuity at the optical trap.

The fact that all the boundary conditions are 0-valued suggests constructing a self-adjoint operator, consistent with these conditions, from the relevant differential operator: ∂_x^4. To do so, we left-multiply the equation of motion by an as-yet arbitrary function $\mathcal{W}_k(x)$ and integrate over the entire domain. Because h is constructed to solve the (linear) equation of motion (Eq. 57), g must as well, and we derive an equation of motion for the quantities $g_k \equiv \int_0^L dx \mathcal{W}_k(x) g(x)$:

$$\frac{1}{\tilde{\nu}} \partial_t g_k = -\int_0^L dx \mathcal{W}_k(x) g_{xxxx} \tag{64}$$

We then integrate the right-hand side by parts. However, we must admit the possibility that g supports a discontinuity in its higher-order derivatives, i.e., $[g_{xxx}(x_p)] \neq 0$. For this reason, we define $\{g^a(x, t), \mathcal{W}^a_k(x)\}$ and $\{g^f(x, t), \mathcal{W}^f_k(x)\}$, as in Eq. 58, defined on the anchored and free sections, respectively. If we choose $\mathcal{W}$ to obey the same homogeneous boundary conditions as g, we eliminate all but four of the surface terms from the integration by parts in Eq. 64), the remaining terms vanish upon choosing $\mathcal{W}$ to obey and $\mathcal{W}(x_p) = 0$ and the same matching conditions as g. We now choose $\mathcal{W}^{\{a,f\}}_k$ to obey the eigenvalue condition $\partial_x^4 \mathcal{W}^{\{a,f\}}_k = k^4 \mathcal{W}^{\{a,f\}}_k$. Because we have constructed a self-adjoint operator, the eigenvalues are real and positive. We are left with $\partial_t g_k = -\tilde{\nu} k^4 g_k$, the solution of which is, as before, $g_k(t) = g_k(0) e^{-\tilde{\nu} k^4 t}$ for $k \neq 0$. Fortunately, the boundary and matching conditions do not admit a solution to $g_{xxxx} = 0$, and we need not consider a 0 mode.

Given some initial condition $y(x, 0)$, we project it onto this strange eigenspace spanned by $\{\mathcal{W}_k\}$. We then construct $g(x, t)$ for all later times in a standard Green's function way,

$$g(x, t) = \int_0^L \frac{dx'}{L} \mathcal{G}(x, x'; t) \left\{ \frac{y(x', 0)}{y_0} - h(x', 0) \right\} \tag{65}$$

where

$$\mathcal{G} = \sum_k e^{-\tilde{\nu} k^4 t} \mathcal{W}_k(x) \mathcal{W}_k(x') \tag{66}$$

and we see that all modes die.

We now solve for the countably infinite sets $\{k\}$ and $\{\mathcal{W}_k\}$. The general solution of $\partial_x^4 \mathcal{W}^{\{a,f\}}_k = k^4 \mathcal{W}^{\{a,f\}}_k$ is

$$\begin{aligned} \mathcal{W}^{\{a,f\}}_k = a_1^{\{a,f\}} \sin(kx) + a_2^{\{a,f\}} \cos(kx) \\ + a_3^{\{a,f\}} \sinh(kx) + a_4^{\{a,f\}} \cosh(kx) \end{aligned} \tag{67}$$

where the eight arbitrary constants will solve the four boundary and four matching conditions. The insertion and elimination of these constants is not a joyful task and will be omitted here. The most important fact is that the set of eight equations for eight unknowns dictates a solvability condition, written explicitly in Appendix D and graphically constructed in Fig. 11, which determines the allowed values of k, given some fixed ratio ρ. The first three normalized eigenfunctions are illustrated in Fig. 12 for $\rho = \frac{1}{2}$.

The complicated solvability condition can be expressed compactly as the separable equation

$$\mathcal{D} = \partial_p F(p) H(q) + F(p) \partial_q H(q) = 0 \tag{68}$$

where $F(p) \equiv \cos(p) \cosh(p) - 1$, $H(q) \equiv \cos(q) \cosh(q) + 1$, $p \equiv k x_p$, and $q \equiv kl$. This differential relation describes the motion along each of the branches shown in the figure as ρ varies, each branch indexed by arbitrary constants introduced upon integrations of Eq. 68, and separated by the singularity lines $\{H = 0, F = 0\}$ at which the differential equation is not invertible. The geometry chosen by the experimenter dictates x_p, l, and therefore $x_p/l = p/q = \rho$. Inspecting the figure, we see that we choose a set of modes

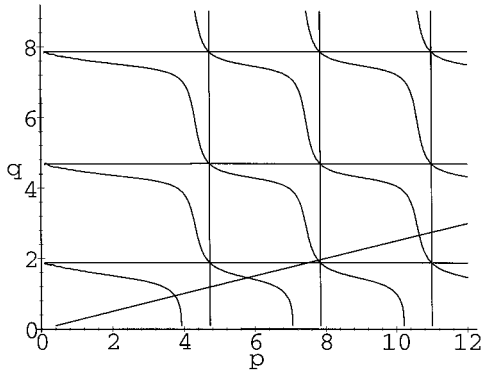

FIGURE 11 $p - q$ plane showing roots of the solvability condition. Here $p \equiv kx_p$ and $q \equiv kl = k(L - x_p)$. The geometry of the experiment dictates ρ, as described in the text. Vertical and horizontal lines correspond to solutions of $F(p) = 0$ and $H(q) = 0$, respectively. The diagonal line indicates the solution to $x_p/L = 0.8$.

by drawing a line of slope ρ through the origin; each intersection with a branch corresponds to one mode.

A further curiosity is that each of the four equations $\{F, H, F_p, H_q\} = 0$ is itself a separate solvability condition associated with a separate experimental geometry. In the language of Appendix D, we may rewrite the condition $\mathcal{D} = 0$, with the first letter below indicating the boundary condition for the left end of one side, and the second for the condition at the right,

$$\mathcal{D} = (cf)(hf) + (ch)(ff) \tag{69}$$

Otherwise stated, the total solvability condition determining relaxation rates for a biopolymer clamped at the left, trapped in the middle, and free at the right is an average of those for 1) the left side clamped at 0 and free at x_p, with the right side hinged at x_p and free at L, and 2) the left side clamped at 0 and hinged at x_p, with the right side free at x_p and free at L.

Armed with a set of decaying modes, we may solve the equation for all times. We now attempt, as in Eq. 50, to construct a polynomial solution that describes the initial data. The polymer initially sits at rest with $y(0) = \Delta$ and is subject to the stated matching and boundary conditions. Noting that the shape must be described by polynomials of less than fourth order, because we wish to describe an elastica experiencing no forces, we find the polynomial $\bar{y}$:

$$\bar{y}^a(\alpha) = \Delta\left(1 - \frac{3}{2}\alpha^2 + \frac{1}{2}\alpha^3\right) \tag{70}$$

$$\bar{y}^f(\sigma) = -\Delta\frac{3\sigma}{2\rho} \tag{71}$$

The final configuration, after the axoneme comes to rest and all transients have died, will be $-\bar{y}$: a third-order polynomial on the left and a straight line on the right. A pleasant fact is that this polynomial can also be derived by taking the limit as $v_c \to 0$ of $y_0 h^{\{a,f\}}$ in Eqs. D1, D2.

We now wish to use this information to arrive at a measurement of A. Hoping to verify the plausibility of this analysis, we compare with the results and accompanying model published with the experiment.

The model presented by Felgner et al. (1996) ignores the left end ($0 < x < x_p$), seeking to describe the dynamics of the free end ($x_p < x < L$), and can be summarized as follows. First, the forces are calculated on a slender body subject to 1) a constant flow and 2) a flow linearly increasing from 0 at the origin to some v_m at the end. The linearly increasing flow describes that experienced by a rigidly rotating rod, approximating the force experienced by the actual (curved) filament. Inexpliciably, different drag coefficients are used for these two forces.

The forces are then used to compute end displacements, using the results for the elastica clamped at the origin. Caveats to this approximation include inconsistency with both the assumption of a rodlike shape and with the experimental geometry, in which the polymer at x_p is neither clamped ($y_x = 0$, as was assumed for the calculation of end displacement) nor hinged ($y_{xx} = 0$, as might be considered appropriate for a straight rod); it is in fact experiencing a torque at x_p due to the side of the filament between the trap and the axoneme.

Summing 1) the end displacement $y_c(v_c; \zeta_1)$ of a clamped elastica in constant flow (using the first drag coefficient) and 2) the end displacement $y_l(v_m; \zeta_2)$ of an elastica subject to the linearly increasing flow it would have experienced were it a rigid rod (using the second drag coefficient), the total deflection y_δ from a straight line is obtained (see equation 20 of Felgner et al., 1996):

$$y_\delta = \frac{\pi\eta(11v_m + 30v_c)l^4}{60A\ln(2l/d)} \tag{72}$$

This end displacement is then used to approximate the deflection that would have been experienced had the filament in the calculation not been initially horizontal, but rather constrained to a nonzero slope at the trap, i.e., that of the $t \to \infty$ solution for the shape, $-\bar{y}$.

This deflection y_δ, from the right tip position at $t = \infty$ to that at $t = \Delta/v_c$, when the axoneme halts, is the first experimental observable. The second is the velocity at this tip at $t = \Delta/v_c$, which is then equated with the maximum velocity v_m in the expression for y_l. Dividing y_δ by the weighted sum of velocities appearing in the numerator, one obtains the combination of two observables (y_δ, v_m) and one experimental parameter (v_c) which, according to this model, is equivalent to a simple quotient with units of time and in which A appears explicitly,

$$\mathcal{T} = \frac{y_\delta}{(11v_m + 30v_c)} = \frac{11\pi\eta l^4}{\text{“}A\text{”}\ 60\ln(2l/d)} \tag{73}$$

where “A” indicates the rigidity that would be extracted from the data using this model. Note that the expression is a function only of l, the length of the free segment of the

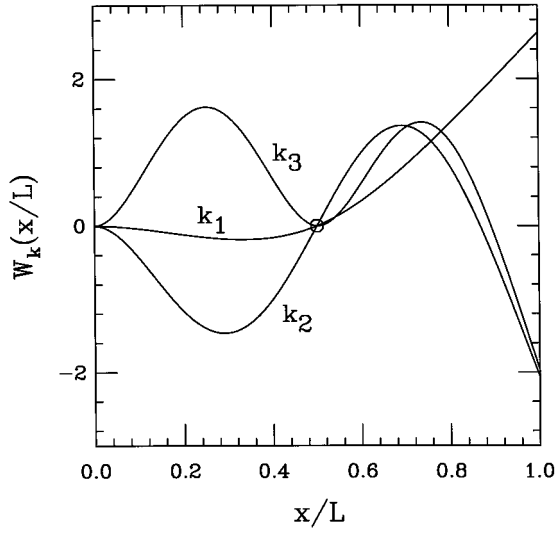

FIGURE 12 The first three modes for the discontinuous EHDI experiment. The circle indicates the pinning point $x_p/L = p/(p + q)$.

polymer. In this model, l is taken to be "the hydrodynamically relevant length" (Felgner et al., 1996).

Returning to the partial differential equation treatment of the problem, we see that the solutions to Eq. 58 for the post-transient polynomial shape relate the velocity of the free end to the constant stage velocity as

$$v_m = v_c h_\tau^f|_{\sigma=1} = \frac{3}{2}\frac{l}{x_p} v_c \tag{74}$$

This simplification allows us to solve for the ratio in Eq. 72 of observables and parameters in terms of the polynomials in Eqs. 71 and D1:

$$\mathcal{T} = \frac{\zeta l^4}{2520A} \frac{(-16\rho^4 + 210\rho^2 + 420\rho + 231)}{(11 + 20\rho)} \tag{75}$$

where A indicates the value of the bending modulus that one would calculate had one used the same data and thus the same quotient $\mathcal{T}$.

The ratio $A/\text{“}A\text{”}$ is a simple expression and allows us to compare the factor by which this differential equation-based analysis differs from the published model, given some experimental data $\mathcal{T}(l)$. Equating the two expressions for $\mathcal{T}$ and isolating $A/\text{“}A\text{,”}$ we find

$$\frac{A}{\text{“}A\text{”}} = 2\frac{\ln\left(\frac{L}{d}\frac{1}{2(1+\rho)}\right)}{\ln\left(\frac{L}{d}\frac{4}{\sqrt{e}}\right)}\left(1 + \frac{210\rho^2 - 16\rho^4}{231 + 420\rho}\right) \tag{76}$$

where we have moved the $\mathcal{O}(1)$ constants into the argument of the logarithm for compactness. The dominant behavior is captured by the polynomial dependence on ρ, but we can see that the function will be ~ 2, indicating a systematic underestimate by the published model of the bending modulus. A plot of the ratio, with typical values taken from experiment, is shown in Fig. 13.

Note that we have arrived at this expression by ignoring the transient component in the exact expression. This is valid only in the range where the polynomial (asymptotic) solution dominates over the transients, a condition that is violated above $\rho \simeq 4$, $x_p/L = \rho/(\rho + 1) \simeq 0.8$.

We expect, then, that results obtained with the model in Felgner et al. (1996) will be comparable, but will systematically underestimate the bending modulus A by a factor of $\sim$½.

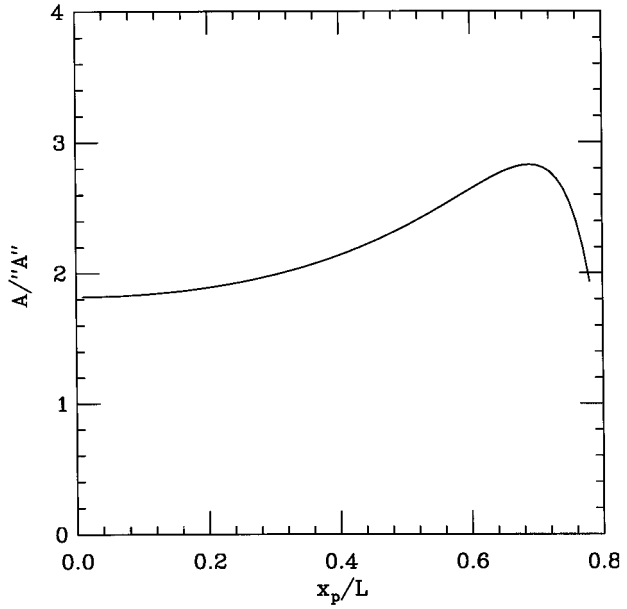

FIGURE 13 Quotient of values derived for the bending modulus using the model of Felgner et al. (1996) and that presented herein.

CONCLUSIONS

We have attempted to show that a systematic treatment of linearized elastohydrodynamics for filamentous biopolymers can be formulated with fruitful results. Furthermore, we have proposed and demonstrated a new technique (EHDII) that exploits viscous hydrodynamics to extend the range of mechanical experiments of bending moduli to more flexible polymers. We expect this experiment to produce more accurate results when repeated with lower-amplitude driving, and thereby help determine conclusively the existence or nonexistence of scale-dependent or time-dependent elastic behaviors in biopolymers as well as the value of bending moduli via in vitro assays. It is our hope that the analysis associated with this experiment will also encourage renewed interest in the problems of flagellar motion and slender-body hydrodynamics in general.

Moreover, we have seen that attentiveness to equations of motion and boundary conditions for the elastica has measurable consequences, and that construction of the appropriate function space associated with these conditions leads to a pleasant union of mathematical and physical intuitions, relating transcendental equations to physical effects and experimental observables. We believe that the significance of boundary conditions and the natural function space for the elastica has been overlooked in existing treatments of the dynamics relevant to experiments being performed and discussed by the community.

We look forward to the extension of this analysis to arbitrary geometries, reflecting distortions beyond small order and hydrodynamics beyond the lowest-order approximation of slender-body flow. Although the exact equation of motion is nonlinear, the Stokesian dynamic and the vanishing of successive derivatives at ends remain, and we expect the mechanisms and effects that we have outlined here to persist.

Natural extensions of this research include nonplanar geometries and the incorporation of twist. These would be complementary to recent work on the Hamiltonian dynamics of twisted elastic rods (Goriely and Tabor, 1997; Olson and Zhurkin, 1996). The dynamics of twist are especially intriguing in light of recent work on twist-bend coupling (Kamien, 1998) and the proposal that this coupling creates

scale-dependent elasticity in actin (Käs et al., 1993). We are currently formulating the analysis appropriate to these promising applications, armed with the lessons learned in this investigation (Wiggins et al., 1997).

APPENDIX A: DIGRESSION ON BOUNDARY CONDITIONS

It is useful to pause momentarily and reflect on the importance of boundary conditions and how they enter into the analysis. To this end, we consider an experiment analogous to EHDI in which the left side of the polymer is hinged rather than clamped. This would be realized by holding the polymer in an optical trap, for example, rather than some torque-exerting anchor like an axoneme fixed to a coverslip. For this experimental setup we replace the boundary condition $h_\alpha(0, \tau) = 0$ with $h_{\alpha\alpha}(0, \tau) = 0$.

Intuitively, we expect the polymer to align itself with the flow as $t \to \infty$ in the absence of any torque at the left end. Mathematically, we may think of the change in boundary conditions via some curious pathologies. The first complication is that there is no time-independent fourth-order polynomial in α that is consistent with the boundary conditions. This prevents us from constructing a static attractor for the problem, as in Eq. 21. However, we note that the equation of motion is solved by a fifth-order, time-dependent polynomial in α:

$$\bar{h}(\alpha, \tau) = \frac{3}{2}(\tau + C)\alpha + \frac{1}{4!}\left(-\alpha^3 + \alpha^4 - \frac{3}{10}\alpha^5\right) \tag{A1}$$

To derive this polynomial, we first express the solution in the form $\Sigma_n c_n(\tau)\alpha^n$. However, as in the derivation following Eq. 59, we expect this solution to depend only linearly on the driving and thus linearly on time. Constraining $\partial_t^2 c_n = 0$ and respecting the relationship between $\partial_\tau c_n$ and c_{n+4} dictated by Eq. 12, we uniquely specify the polynomial up to the constant C.

The fact that our long-time solution contains an arbitrary constant should lead us to rethink splitting the solution into a polynomial and a set of only-decaying modes. Returning to the set of eigenvalues of ∂_α^4, we discover a second complication for this new boundary condition: there now exists a zero mode—a nontrivial solution, consistent with the boundary conditions, to the equation $\partial_\alpha^4 \mathcal{W}_0 = 0$, i.e., the normalized polynomial $\sqrt{3}\alpha$. We then may choose C to eliminate the overlap of $\mathcal{W}_0$ with the initial data, i.e., $0 = g_0 = \langle g|\mathcal{W}_0\rangle = \langle h(\alpha, 0)|\mathcal{W}_0\rangle - \langle \bar{h}(\alpha)|\mathcal{W}_0\rangle$.

We now see how the change in boundary conditions creates drastically different physical behavior. The long-time solution contains a term describing a straight line whose slope grows with velocity $3u/2L$ without bound.

To illustrate further the relationship between a change in boundary conditions and the qualitative behavior, note that the dynamics, even in the presence of an inhomogeneous equation of motion, can be cast in terms of the functional derivative of an energy:

$$h_\tau = -\frac{\delta \mathcal{F}}{\delta h(\alpha)}$$
$$\mathcal{F} = \int_0^1 d\alpha' \left[-h + \frac{1}{2}(h_{\alpha\alpha})^2\right] \tag{A2}$$

The first term represents the drag force acting in the positive y direction, and the second is simply the nondimensionalization of the elastic bending energy term from which we originally derived the equation of motion. We then find

$$\mathcal{F}_\tau = \int_0^1 d\alpha h_\tau \frac{\delta \mathcal{F}}{\delta h(\alpha)} = -\int_0^1 d\alpha (h_\tau)^2 \tag{A3}$$

indicating that $\mathcal{F}$ is a monotonically decreasing function in time (Cross and Hohenberg, 1993).

We must now only show that for the clamped (hinged) polymer this energy functional is (is not) bounded from below. Rewriting $h = \Sigma c_n(\tau)\alpha^n$, we can evaluate the energy explicitly as

$$\mathcal{F} = -\sum_{n=0}^{\infty} \frac{c_n}{n+1} + \mathcal{R} \tag{A4}$$

where

$$\mathcal{R} = \frac{1}{2}\sum_{m,n=2}^{\infty} \frac{n(n-1)m(m-1)}{n+m-3} c_m c_n \tag{A5}$$

If $h(0) = h_x(0) = 0$, $c_0 = c_1 = 0$, and the sum in Eq. A4 runs from 2 to ∞. We see that we cannot simply make $\mathcal{F}$ arbitrarily negative by introducing a large and positive c_j for some j, because this term will appear quadratically (and always positively) in the second term. However, replacing the condition $h_\alpha(0) = 0$ with $h_{\alpha\alpha}(0) = 0$ changes the condition $c_1 = 0$ to $c_2 = 0$; c_1 appears in the first term in Eq. A4, but not the second. Now the energy can become arbitrarily negative if $c_1 = h'(0)$ becomes arbitrarily positive. A divergent slope simply means the curve points straight up, in accord with our intuition for the long-time behavior of a polymer free to rotate in some background flow. Note such a long-time behavior means leaving the small-h_x limit for which the dynamic was originally derived.

APPENDIX B: EIGENFUNCTIONS OF ∂_α^4

If we equate functions related by the reflection $\alpha \to 1 - \alpha$, there are $4(4 + 1)/2 = 10$ distinct eigenfunctions of ∂_α^4, determined by boundary conditions, for which this operator is self-adjoint. Each has an associated solvability condition for the eigenvalues k. We list the solvability conditions and the unnormalized eigenfunctions, indexed according to the conditions at the ends:

$$(f) \text{ free:} \quad h_{xx} = h_{xxx} = 0$$
$$(c) \text{ clamped:} \quad h = h_x = 0$$
$$(h) \text{ hinged:} \quad h = h_{xx} = 0$$
$$(t) \text{ torqued:} \quad h_{xxx} = h_x = 0$$

The general solution is $\mathcal{W}_k = a_1 \cos k\alpha + a_2 \sin k\alpha + a_3 \cosh k\alpha + a_4 \sinh k\alpha$, where $\alpha \in (0, 1)$. The letters f, c, h, t denote the boundary conditions at the left and right.

Note that for three special cases, the calculated $\mathcal{W}_k$ are merely a Fourier basis. The solvability condition for the f-f and f-c cases appear in Landau and Lifshitz (1986, Sect. 25, problems 4 and 6). If we differentiate the c-c expression and define $\alpha_n = k_n/2$, then we recover equation 28 of Gittes et al. (1993). The expansion in terms of k has the advantage of a single solvability condition $\cos(k_n)\cosh(k_n) = 1$, rather than the two conditions $\tanh(\alpha_n) = (-1)^n \tan(\alpha_n)$. The latter two conditions may be derived from the former via half-angle formulae.

$f-f$:

$$\cos k \cosh k = 1;$$
$$\mathcal{W}_k = (\sin k\alpha + \sinh k\alpha)(\sin k + \sinh k) + (\cos k\alpha + \cosh k\alpha)(\cos k - \cosh k) \tag{B1}$$

$c - c$:

$$\cos k \cosh k = 1;$$
$$\mathcal{W}_k = (\sin k\alpha - \sinh k\alpha)(\sin k + \sinh k) + (+\cos k\alpha - \cosh k\alpha)(\cos k - \cosh k) \tag{B2}$$

$f - c$:

$$\cos k \cosh k = -1;$$
$$\mathcal{W}_k = (\sin k\alpha + \sinh k\alpha)(\sin k - \sinh k) + (\cos k\alpha + \cosh k\alpha)(\cos k + \cosh k) \tag{B3}$$

$h - h$:

$$\sin k = 0;$$
$$\mathcal{W}_k = \sin k\alpha \tag{B4}$$

$t - t$:

$$\sin k = 0;$$
$$\mathcal{W}_k = \cos k\alpha \tag{B5}$$

$h - t$:

$$\cos k = 0;$$
$$\mathcal{W}_k = \sin k\alpha \tag{B6}$$

$f - h$:

$$\tan k = \tanh k;$$
$$\mathcal{W}_k = (\sin k\alpha + \sinh k\alpha)(-\cos k + \cosh k) + (\cos k\alpha + \cosh k\alpha)(\sin k - \sinh k) \tag{B7}$$

$f - t$:

$$\tan k = -\tanh k;$$
$$\mathcal{W}_k = (\sin k\alpha + \sinh k\alpha)(\sin k + \sinh k) + (\cos k\alpha + \cosh k\alpha)(\cos k - \cosh k) \tag{B8}$$

$c - t$:

$$\tanh k = -\tanh k;$$
$$\mathcal{W}_k = (\sin k\alpha - \sinh k\alpha)(\sin k + \sinh k) + (\cos k\alpha - \cosh k\alpha)(\cos k - \cosh k) \tag{B9}$$

$c - h$:

$$\tan k = \tanh k;$$
$$\mathcal{W}_k = (\sin k\alpha - \sinh k\alpha)(\cos k + \cosh k) + (-\cos k\alpha + \cosh k\alpha)(\sin k + \sinh k) \tag{B10}$$

APPENDIX C: EXACT SOLUTION TO EHD PROBLEM II

The exact solution to EHDII can be written in somewhat compact form at the cost of introducing new definitions. Employing the coordinate $\alpha \equiv x/L$, the rescaled length $\mathcal{L} \equiv L/\ell$, and the constant $z_0 = \exp(-i\pi/8)$ as in the text (Elastohydrodynamic Problem II), we introduce $\xi \equiv \exp(z_0\mathcal{L})$ and then write

$$h(\alpha, \mathcal{L}) \equiv h_\infty(\alpha) + h_b(\alpha, \mathcal{L}) \tag{C1}$$

where h_∞ is the semiinfinite solution, and $h_b \to 0$ as $\mathcal{L} \to \infty$. Explicitly,

$$h_b = \frac{1}{2} C_1(\xi^\alpha - \xi^{-\alpha}) + \frac{1}{2} C_2(\xi^{i\alpha} - \xi^{-i\alpha}) \tag{C2}$$

where

$$C_1(\mathcal{L}) = \xi^{-1} \frac{(-i\xi^{-i} - \xi^i + (1+i)\xi)}{(i\xi^{-1-i} + \xi^{-1+i} - \xi^{1-i} - i\xi^{1+i})} \tag{C3}$$

$$C_2(\mathcal{L}) = \xi^{-i} \frac{(i\xi^{-1} - \xi^1 + (1-i)\xi^i)}{(-i\xi^{-1-i} - \xi^{-1+i} + \xi^{1-i} + i\xi^{1+i})}$$

and

$$h_\infty = \frac{1}{2}(\xi^{-\alpha} + \xi^{-i\alpha}) \tag{C4}$$

APPENDIX D: SOLVABILITY CONDITION FOR DISCONTINUOUS EHDI

Associated with the discontinuous EHDI problem are the solutions to Eq. 58 satisfying the inhomogeneous boundary conditions. These solutions may be written as polynomials on the left and right sides of the trap:

$$h^f\rho^5 = -\frac{1}{80}\sigma^5 - \frac{1}{24}\rho\sigma^4 + \left(\frac{\rho}{6} + \frac{1}{8}\right)\sigma^3 - \frac{1}{4}(\rho+1)\sigma^2 + \left(\frac{1}{105}\rho^4 - \frac{1}{8}\rho^2 - \frac{1}{8}\rho + \frac{3}{2}\rho^4\tau\right)\sigma \tag{D1}$$

$$h^a\rho^3 = \frac{1}{1680}\alpha^7\rho^3 - \frac{1}{240}\alpha^6\rho^3 - \tau\rho^3 + \left(\frac{13}{560}\rho^3 - \frac{1}{8}\rho - \frac{1}{8} - \frac{1}{2}\rho^3\tau\right)\alpha^3 + \left(-\frac{11}{560}\rho^3 + \frac{1}{8}\rho + \frac{1}{8} + \frac{3}{2}\rho^3\tau\right)\alpha^2 \tag{D2}$$

The notation and matching conditions are described in the text (The Discontinuous EHDI Experiment).

The homogeneous boundary conditions are solved by an expansion in a specially constructed set of piecewise-defined orthonormal eigenfunctions of ∂_x^4 with associated eigenvalues appropriate to the boundary and matching conditions. Like the statement $\sin(kL) = 0$ for determining the allowed Fourier k values for a doubly hinged filament of length L, there is a solvability condition for $p \equiv kx_p$, $q \equiv k(L - x_p) = kl$, derived by setting

the determinant of an 8×8 matrix to 0, an equation that can be written

$$\begin{aligned} 0 = \mathcal{D}(p, q) = \\ &-\sin(q)\cos(p)\cosh(q)\cosh(p) \\ &- \cos(q)\sin(p)\cosh(q)\cosh(p) \\ &+ \cos(q)\cos(p)\sinh(q)\cosh(p) \\ &+ \cos(q)\cos(p)\cosh(q)\sinh(p) \\ &- \sin(q)\cosh(q) + \cos(q)\sinh(q) \\ &+ \sin(p)\cosh(p) - \cos(p)\sinh(p) \end{aligned} \tag{D3}$$

The ratio $x_p/(L - x_p) = q/p = \rho$, set by the geometry of the experiment, fixes a diagonal line passing through the origin and intersecting the set of curves defined by this equation to define all of the allowed k values, as illustrated in Fig. 11.

We thank Steve Block and Steve Gross for early discussions on analysis of the data and for bringing Felgner et al. (1996) to our attention, and Joseph Käs for pointing out Gittes et al. (1993). We also thank Almut Bruchard, Mark Johnson, Frank Jülicher, Randall Kamien, David Levermore, Mike Shelley, and especially Tom Powers for useful conversations and insight.

This work was supported by National Science Foundation PFF grant DMR 93-50227 and the A. P. Sloan Foundation (REG).

REFERENCES

Amblard, F., A. C. Maggs, B. Yurke, A. N. Pargellis, and S. Leibler. 1996. Subdiffusion and anomalous local viscoelasticity in actin networks. *Phys. Rev. Lett.* 77:4470–4473.

Barkley, M., and B. Zimm. 1978. Theory of twisting and bending of chain macromolecules: analysis of the fluorescence depolarization of DNA. *J. Chem. Phys.* 70:2991–3007.

Childress, S. 1981. Swimming and Flying in Nature. Cambridge University Press, Cambridge.

Cluzel, P., A. Lebrun, C. Heller, R. Lavery, J. L. Viovy, D. Chatenay, and F. Caron. 1996. DNA: an extensible molecule. *Science.* 271:792–794.

Cox, R. 1970. The motion of long slender bodies in a viscous fluid. Part I. General theory. *J. Fluid Mech.* 44:791–810.

Cox, R. 1971. The motion of long slender bodies in a viscous fluid. Part II. Shear flow. *J. Fluid Mech.* 45:625–657.

Cross, M. C., and P. C. Hohenberg. 1993. Pattern formation outside of equilibrium. *Rev. Modern Phys.* 65:851–1112.

Doi, M., and S. F. Edwards. 1986. The Theory of Polymer Dynamics. Clarendon Press, Oxford.

Felgner, H., R. Frank, and M. Schliwa. 1996. Flexural rigidity of microtubules measured with the use of optical tweezers. *J. Cell Sci.* 109: 509–516.

Fixman, M. 1978. Simulation of polymer dynamics. I. General theory. *J. Chem. Phys.* 69:1527–1537.

Gittes, F., B. Mickey, J. Nettleton, and J. Howard. 1993. Flexural rigidity of microtubules and actin filaments measured from thermal fluctuations in shape. *J. Cell. Biol.* 120:923–934.

Goldstein, R., and S. Langer. 1995. Nonlinear dynamics of stiff polymers. *Phys. Rev. Lett.* 75:1094–1097.

Goriely, A., and M. Tabor. 1997. Nonlinear dynamics of filaments. *Physica D.* 105:20–61.

Harris, R. A., and J. E. Hearst. 1966. On polymer dynamics. *J. Chem. Phys.* 44:2595–2602.

Isambert, H., and A. Maggs. 1996. Dynamics and rheology of actin solutions. *Macromolecules.* 29:1036–1040.

Kamien, R. 1998. Local writhing dynamics. *Euro. Phys. J. B.* (in press).

Käs, J., H. Strey, M. Baermann, and E. Sackmann. 1993. Direct measurement of the wave-vector-dependent bending stiffness of freely flickering actin filaments. *Europhys. Lett.* 21:865–870.

Keller, J., and S. Rubinow. 1976. Slender-body theory for slow viscous flow. *J. Fluid Mech.* 75:705–714.

Kurachi, M., M. Hoshi, and H. Tashiro. 1995. Buckling of a single microtubule by optical trapping forces: direct measurement of microtubule rigidity. *Cell Motil Cytoskeleton.* 30:221–228.

Landau, L., and L. Lifshitz. 1986. Theory of Elasticity. Pergamon, New York.

Landau, L., and L. Lifshitz. 1987. Fluid Mechanics. Pergamon, New York. 59.

Lighthill, J. 1975. Mathematical Biofluiddynamics. SIAM, Philadelphia.

Love, A. E. H. 1892. A Treatise on the Mathematical Theory of Elasticity. Cambridge University Press, Cambridge.

Machin, K. E. 1958. Wave propagation along flagella. *J. Exp. Biol.* 35:796–806.

Machin, K. E. 1962. The control and synchronization of flagellar movement. *Proc. R. Soc. Lond. B* 62:88–104.

MacKintosh, F., and P. A. Janmey. 1997. Actin gels. *Curr. Opin. Solid State Mater. Sci.* 2:350–367.

Mendelson, N. H. 1990. Bacterial macrofibers: the morphogenesis of complex multicellular bacterial forms. *Sci. Prog. Oxford.* 74:425–441.

Olson, W. K., and V. B. Zhurkin. 1996. Twenty years of DNA bending. *In* Biological Structure and Dynamics, Vol. 2. R. H. Sarma and M. H. Sarma, editors. Adenine Press, Schenectady, NY. 341–370.

Ott, A., M. Magnasco, A. Simon, and A. Libchaber. 1993. Measurement of the persistence length of polymerized actin using florescence microscopy. *Phys. Rev. E.* 48:1642–1645.

Purcell, E. M. 1977. Life at low Reynolds number. *Am. J. Phys.* 45:3–11.

Riveline, D., C. H. Wiggins, R. E. Goldstein, and A. Ott. 1997. Elastohydrodynamic study of actin filaments using fluorescene microscopy. *Phys. Rev. E.* 56:1330–1334.

Shapere, A., and F. Wilczek. 1987. Self-propulsion at low Reynolds number. *Phys. Rev. Lett.* 58:2051–2053.

Shelley, M. J., and T. Ueda. 1996. The nonlocal dynamics of stretching, buckling filaments. *In* Advances in Multi-fluid Flows. Y. Y. Renardy, A. V. Coward, D. T. Papageorgiou, and S-M Sun, editors. AMS-SIAM, Philadelphia. 415–425.

Smith, S. B., Y. Cui, and C. Bustamante. 1996. Overstretching B-DNA: the elastic response of individual double-stranded and single-stranded DNA molecules. *Science.* 271:795–799.

Stokes, G. G. 1851. Mathematical and Physical Papers. III. Cambridge University Press, Cambridge. 19, 130.

Taylor, G. 1952. The action of waving cylindrical tails in propelling microscopic organisms. *Proc. R. Soc. Lond. A* 217:225–239.

Vernier, P., A. C. Maggs, M.-F. Carlier, and D. Pantaloni. 1994. Analysis of microtubule rigidity using hydrodynamic flow and thermal fluctuations. *J. Biol. Chem.* 269:13353–13360.

Weinstock, R. 1974. Calculus of Variations. Dover, New York.

Wiggins, C. H., T. R. Powers, and R. E. Goldstein. 1997. Supercoiling dynamics at low Reynolds numbers. (preprint).

Yin, H., M. D. Wang, K. Svoboda, S. M. Block, and J. Gelles. 1995. Transcription against an applied force. *Science.* 270:1653–1657.